Engineering Structures 266 (2022) 114618

Contents lists available at ScienceDirect

Engineering Structures

journal homepage: www.elsevier.com/locate/engstruct

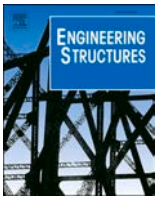

The equilibrium and form-finding of general tensegrity systems with rigid bodies

Shuo Ma [a,b], Muhao Chen [c,*], Zhangli Peng [d], Xingfei Yuan [e,*], Robert E. Skelton [c]

[a] College of Civil Engineering, Zhejiang University of Technology, Hangzhou, Zhejiang 310023, China
[b] Key Laboratory of Space Structures of Zhejiang Province, Hangzhou, Zhejiang 310058, China
[c] Department of Aerospace Engineering, Texas A & M University, College Station, TX 77840, United States
[d] Department of Biomedical Engineering, University of Illinois at Chicago, Chicago, IL 60607, United States
[e] College of Civil Engineering and Architecture, Zhejiang University, Hangzhou, Zhejiang 310058, China

ARTICLE INFO

Keywords:
Generalized tensegrity
Rigid body
Tensegrity equilibrium
Minimal coordinate
Form-finding

ABSTRACT

We develop a general approach to study the equilibrium and form-finding of any general tensegrity systems with rigid bodies. The equilibrium equations are derived in an explicit form in terms of a nodal coordinate and orientation parameter as the minimal coordinate. The nodal vector consists of nodes (either free or pinned) in the pure bar-string tensegrity network and nodes on the rigid bodies (those connected to the pure bar-string tensegrity network). Based on the Lagrangian method, the nonlinear statics of the general tensegrity system in terms of the minimal coordinate is first given. Then, we linearize the statics equation and obtain its equivalent form, in terms of the force vector of the compressive and tensile members, to analyze structure equilibrium configurations and prestress modes. To study the system's stability and have a comprehensive insight into the materials and structure members, we present the tangent stiffness matrix as a combination of the structure's prestress, material, and geometric information. It is also shown that without rigid bodies, the governing equations of the general tensegrity system yield to the classical tensegrity structure (pure string-bar network). Form-finding of general tensegrity is implemented based on solving the nonlinear equilibrium equation, where the modification of tangent stiffness matrix and line search algorithm is used. Numerical examples demonstrate the capability of our developed method in finding the feasible prestress modes, conducting form-finding and prestress designs, and checking the structural robustness of any tensegrity systems with rigid bodies.

1. Introduction

Tensegrity is a conjunction of two words (tension and integrity) which was first proposed by Buckminster Fuller [1] for the art form by Ioganson (1921) and Snelon (1948) [2]. In their work, they never assumed there were no rigid bodies in the tensegrity structures. And in fact, the tensegrity sculpture built by Snelson in 1948 is two X-shape rigid bodies stabilized by several cables. However, it is probably because bars and strings are more efficient in taking compression, provide more accurate models (uncertainty is only along with the axially loaded members), and it is complicated to model the irregular shape of the rigid bodies, most of the literature focus on pure stable bar-strings networks.

Indeed, after decades of study, the pure bar-string tensegrity structures have shown their many advantages in lightweight structure topology design [3–6], engineering structures [5,7,8], soft robotics [9,10], deployable structures [11–13], energy absorption [14–16], metamaterials [17–19], etc. But for many engineering structures, we must include the rigid bodies, i.e., the deck of the bridges, the roof of the shelters, the shell of cable domes, the D-section of the airfoils, and the shield of space structures. To deal with these rigid bodies in their tensegrity structure design, many researchers have proposed their compromised solutions to the rigid body tensegrities. For example, Carpentieri et al. [20] separated the minimal mass design of the tensegrity bridge structure and its deck. Laccone et al. [21] analyzed the cable-tensioned dome and its glass shell by the nonlinear finite element analysis software Straus7. Levin et al. [22] studied the rigid body spine mechanics based on the tensegrity-truss model. Chen and Jiang [23] used parallel mechanism theory to compute the stiffness of a fish made of rigid ribs stabilized by strings. Chen et al. [24] decoupled the force analysis of a tensegrity space habitat and its shield. However, none of

* Corresponding authors.
E-mail address: muhaochen@tamu.edu (M. Chen).

https://doi.org/10.1016/j.engstruct.2022.114618
Received 12 February 2022; Received in revised form 15 May 2022; Accepted 30 June 2022
Available online 11 July 2022

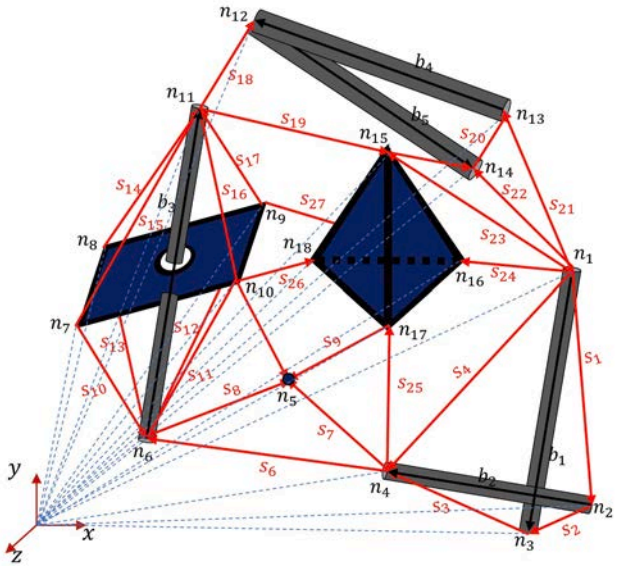

Fig. 1. Diagram of tensegrity with rigid bodies, bar(b) and string(s) vectors are marked in black and red.

these approaches started from the fundamental governing equations of the whole system and developed a general approach to the analysis of tensegrity systems with rigid bodies. It is also worth mentioning that few software packages have the compatibility of simulating tensegrity systems with rigid bodies. For example, Wang et al. [25] modeled tensegrity swimmer and rigid bodies in the MuJoCo simulator and studied the data-based control methods. Sun et al. [26] studied a tensegrity foot with a rigid board and universal joint in ADAMS. Pajunen et al. [16] implemented ABAQUS to analyze the 3D-printable tensegrity lander with rigid joints. However, these commercial packages are costly, require much experience, and the insight of the algorithm is not clear.

In the past years, a few attempts have been made to study tensegrity with rigid body models analytically. For example, for the static analysis, Hangai and Wu [27] proposed kinematics and equilibrium equations to study the behaviors of a hybrid structure that consists of cables and rigid structures. Wang et al. [28] derived the statics equilibrium equation of general tensegrity and used the mixed-integer linear programming method for the topology design. Chen and Jiang [29] derived the total stiffness of a general tensegrity structure in an explicit form and developed a set of sufficient and necessary conditions to guarantee the stability of the tensegrity structures. For the dynamics analysis, Nagase and Skelton [30] used non-minimal coordinates to write the dynamics equations of tensegrity by assuming the compression members are rigid bodies. Kan et al. [31,32] studied the nonlinear dynamics of clustered tensegrity with rigid bodies by using the configuration of the attached rigid bodies as the generalized coordinate. Li et al. [33] studied the kinodynamic planning of cable-driven tensegrity manipulators composed of clustered cables and rigid bodies. However, the equilibrium theory in most of the work is in a complicated form and limited to structures with small deformations.

Moreover, there is increasing interest in using tensegrity structures to build robotics due to the many advantages of tensegrity structure, i.e., mass saving, control energy efficiency, abundant equilibrium states, etc. In many tensegrity robot applications, rigid bodies cannot be avoided. The current equilibrium theories and form-finding methods of the tensegrity system with rigid bodies are still limited. It is critical to have an efficient form-finding approach to find the configurations of the whole system to enlarge the applications of tensegrity systems. To this end, we derived a general approach to the nonlinear equilibrium equations and proposed a corresponding form-finding method to the tensegrity system with rigid bodies. In this study, the tensegrity with pure axial form elements is referred to as the traditional tensegrity, while the tensegrity with rigid bodies is called the general tensegrity.

The paper is structured as follows. Section 2 presents the tensegrity and rigid body notations. Section 3 derives the kinematics of the system. Section 4 gives the nonlinear and linearized statics equations. Section 5 shows the form-finding approach to the tensegrity systems with rigid bodies. Section 6 summarizes the conclusions.

2. Notations of tensegrity systems with rigid bodies

2.1. Nodal coordinates of the system and its components

The tensegrity system with rigid bodies is composed of bars, strings, and rigid bodies, as shown in Fig. 1. The rigid bodies in the tensegrity structures are connected by the strings and bars nodes on the rigid bodies. We name the nodes on the rigid body as rigid body nodes. The nodes only on the bars and strings are free tensegrity nodes, and the other nodes in the fixed point are the pinned tensegrity nodes. The position of all the nodes can be expressed in any frame, and we choose to label them in the Cartesian coordinates in an inertially fixed frame by a nodal vector. Assume there are n_n number of nodes, the X, Y, and Z-coordinates of the i th node $\boldsymbol{n}_i \in \mathbb{R}^3$ in the vector form is $\boldsymbol{n}_i = [x_i \quad y_i \quad z_i]^T$. By stacking $\boldsymbol{n}_i$ for $i = 1, 2, \cdots, n_n$ together, we can get the nodal vector $\boldsymbol{n} \in \mathbb{R}^{3n_n}$ for the whole structure:

$$\boldsymbol{n} = \begin{bmatrix} \boldsymbol{n}_1^T & \boldsymbol{n}_2^T & \cdots & \boldsymbol{n}_{n_n}^T \end{bmatrix}^T, \tag{1}$$

and its equivalent matrix form [34] $\boldsymbol{N} \in \mathbb{R}^{3\times n_n}$ is:

$$\boldsymbol{N} = [\boldsymbol{n}_1 \quad \boldsymbol{n}_2 \quad \cdots \quad \boldsymbol{n}_{n_n}]. \tag{2}$$

Note that one can simply obtain the nodal coordinate vector $\boldsymbol{n}$ by vectorizing the nodal coordinate matrix $\boldsymbol{N}$:

$$\boldsymbol{n} = vec(\boldsymbol{N}) = \boldsymbol{N}(:), \tag{3}$$

where $vec(\boldsymbol{N})$ is an operator that stacks all the columns of matrix $\boldsymbol{N}$ into one vector. Usually, the positions of some of the nodes in the structure are fixed/pinned in specific directions. Let there be n_a degree of freedom of free tensegrity nodes, n_b degree of freedom of pinned tensegrity nodes, and m rigid bodies with a total number of n_q degree of freedom of the rigid nodes. Suppose there are z_i number of nodes in the i th rigid body. To deal with the constraints, we distinguish the free tensegrity nodes, pinned tensegrity nodes, and the jth node in the ith rigid body by introducing three kinds of vectors $\boldsymbol{a} \in \mathbb{R}^{n_a}$, $\boldsymbol{b} \in \mathbb{R}^{n_b}$, and $\boldsymbol{q}_{ij} \in \mathbb{R}^{n_q}$:

$$\boldsymbol{a} = \begin{bmatrix} a_1 & a_2 & \cdots & a_{n_a} \end{bmatrix}^{\mathrm{T}}, \tag{4}$$

$$\boldsymbol{b} = \begin{bmatrix} b_1 & b_2 & \cdots & b_{n_b} \end{bmatrix}^{\mathrm{T}}, \tag{5}$$

$$\boldsymbol{q}_{ij} = \begin{bmatrix} q_{ijx} & q_{ijy} & q_{ijz} \end{bmatrix}^{\mathrm{T}}, \ (i = 1, 2, \cdots, m; \ j = 1, 2, \cdots, z_i), \tag{6}$$

where the values of $a_\alpha(\alpha = 1,2,\cdots,n_a)$, $b_\beta(\beta = 1, 2, \cdots, n_b)$ and q_{ijx}, q_{ijy}, $q_{ijz}(i = 1, 2, \cdots, m; j = 1, 2, \cdots, z_i)$ are the indices of the entries corresponding to the free tensegrity nodes, pinned tensegrity nodes, and the X, Y, Z freedom of the jth node in the ith rigid body in the nodal vector $\boldsymbol{n}$. We use vectors $\boldsymbol{n}_a$, $\boldsymbol{n}_b$, and $\boldsymbol{n}_{q_{ij}}$ to label the nodal coordinate of the free node, pinned node, and the jth node in the ith rigid body. And $\boldsymbol{E}_{na} \in \mathbb{R}^{3n_n\times n_a}$, $\boldsymbol{E}_{nb} \in \mathbb{R}^{3n_n\times n_b}$, and $\boldsymbol{E}_{n_{qij}} \in \mathbb{R}^{3n_n\times 3}$ are the location matrices to extract vectors $\boldsymbol{n}_a$, $\boldsymbol{n}_b$, and $\boldsymbol{n}_{q_{ij}}$ from the vector $\boldsymbol{n}$:

$$\begin{aligned} &\boldsymbol{E}_{na}(:,k) = \boldsymbol{I}_{3n_n}(:,a_k), \boldsymbol{E}_{nb}(:,k) = \boldsymbol{I}_{3n_n}(:,b_k), \boldsymbol{E}_{n_{qij}} = \boldsymbol{I}_{3n_n}\big(\\ &\quad :, \begin{bmatrix} q_{ijx} & q_{ijy} & q_{ijz} \end{bmatrix} \big), \end{aligned} \tag{7}$$

where $\boldsymbol{I}_{3n_n}$ is the identity matrix in $3n_n$ order. Thus, we have the following:

$$\boldsymbol{n_a} = \boldsymbol{E}_{na}^T\boldsymbol{n}, \boldsymbol{n_b} = \boldsymbol{E}_{nb}^T\boldsymbol{n}, \boldsymbol{n}_{q_{ij}} = \boldsymbol{E}_{n_{qij}}^T\boldsymbol{n}. \tag{8}$$

The nodal coordinate of the whole structure is obtained by summing all the free tensegrity nodes, pinned tensegrity nodes, and rigid body nodes:

$$\boldsymbol{n} = \boldsymbol{E}_{na}\boldsymbol{n}_a + \boldsymbol{E}_{nb}\boldsymbol{n}_b + \sum\nolimits_{j=1}^{m}\sum\nolimits_{k=1}^{z_i}\boldsymbol{E}_{n_{qij}}\boldsymbol{n}_{q_{ij}}. \tag{9}$$

The i th ($i = 1,2,\cdots,m$) rigid body nodal coordinate vector is obtained by stacking the nodal coordinate of the z_i rigid-body nodes:

$$\boldsymbol{n}_{q_i} = \begin{bmatrix} \boldsymbol{n}_{q_{i1}} \\ \boldsymbol{n}_{q_{i2}} \\ \vdots \\ \boldsymbol{n}_{q_{iz_i}} \end{bmatrix}. \tag{10}$$

The location matrix corresponding to the i th ($i = 1,2,\cdots,m$) rigid body nodes is:

$$\boldsymbol{E}_{n_{qi}} = \begin{bmatrix} \boldsymbol{E}_{n_{qi1}} & \boldsymbol{E}_{n_{qi2}} & \cdots & \boldsymbol{E}_{n_{qiz_i}} \end{bmatrix}. \tag{11}$$

Then, the nodal coordinate vector of the i th ($i = 1,2,\cdots,m$) rigid body can be calculated by:

$$\boldsymbol{n}_{q_i} = \boldsymbol{E}_{n_{qi}}^T\boldsymbol{n}. \tag{12}$$

2.1.1. Connectivity matrix

A connectivity matrix provides the connection pattern of all the nodes in the structure. Let $\boldsymbol{C} \in \mathbb{R}^{n_e \times n_n}$ be the connectivity matrix of the tensegrity systems with rigid bodies, where n_e is the total number of axially loaded members (bars and strings). The i th ($i = 1,2,\cdots,n_e$) row of $\boldsymbol{C}$, denoted as $\boldsymbol{C}_i = [\boldsymbol{C}]_{(i,:)} \in \mathbb{R}^{1\times n_n}$, represents connectivity information of the i th element in the structure. Suppose the i th member is from the j th node to the k th node. The r th ($i = 1,2,\cdots,n_n$) entry the i th row of $\boldsymbol{C}$ satisfies:

$$[\boldsymbol{C}]_{ir} = \begin{cases} -1, & r = j \\ 1, & r = k \\ 0, & r = else \end{cases}. \tag{13}$$

2.1.2. The geometry of axial elements

An axial element vector denotes the start and end nodes of an axial element (bar or string). For example, the i th axial element vector $\boldsymbol{h}_i \in \mathbb{R}^{3\times 1}$ is:

$$\boldsymbol{h}_i = \boldsymbol{n}_k - \boldsymbol{n}_j = \boldsymbol{C}_i \bigotimes \boldsymbol{I}_3\boldsymbol{n}, \tag{14}$$

where the symbol $\bigotimes$ represents the Kronecker product. Stacking all the axial elements into a structure element matrix $\boldsymbol{H} \in \mathbb{R}^{3\times n_e}$, we get:

$$\boldsymbol{H} = \boldsymbol{N}\boldsymbol{C}^T. \tag{15}$$

The present length of the i th axial element is:

$$l_i = \|\boldsymbol{h}_i\| = \left(\boldsymbol{n}^T\left(\boldsymbol{C}_i^T\boldsymbol{C}_i\right) \otimes \mathbf{I}_3\boldsymbol{n}\right)^{\frac{1}{2}}. \tag{16}$$

Rest length is the length of an axial element with no tension or compression. We use the subscript 0 to denote the rest length of an axial element, i.e., the rest length of the i th axial element is $\boldsymbol{l}_{0i}$. The length and rest length vector of all the axial elements are:

$$\boldsymbol{l}_0 = \begin{bmatrix} l_{01} & l_{02} & \cdots & l_{0n_e} \end{bmatrix}^T, \tag{17}$$

$$\boldsymbol{l} = \begin{bmatrix} l_1 & l_2 & \cdots & l_{n_e} \end{bmatrix}^T. \tag{18}$$

2.1.3. Stiffness of axial elements

Let the cross-sectional area, secant modulus, and tangent modulus of the i th element be A_i, E_i, and E_{ti}, respectively. Then, the cross-sectional area, secant modulus, and tangent modulus vector of the structure $\boldsymbol{A}, \boldsymbol{E}, \boldsymbol{E}_t \in \mathbb{R}^{n_e}$ can be written as:

$$\boldsymbol{A} = \begin{bmatrix} A_1 & A_2 & \cdots & A_{n_e} \end{bmatrix}^T, \tag{19}$$

$$\boldsymbol{E} = \begin{bmatrix} E_1 & E_2 & \cdots & E_{n_e} \end{bmatrix}^T, \tag{20}$$

$$\boldsymbol{E}_t = \begin{bmatrix} E_{t1} & E_{t2} & \cdots & E_{tn_e} \end{bmatrix}^T. \tag{21}$$

The internal force of the i th element is $t_i = A_i\sigma_i = E_iA_i(l_i - l_{0i})/l_{0i}$, the internal force vector of the structure $\boldsymbol{t} \in \mathbb{R}^{n_e}$ can be written as:

$$\boldsymbol{t} = \begin{bmatrix} t_1 & t_2 & \cdots & t_{n_e} \end{bmatrix}^T = \widehat{\boldsymbol{E}}\widehat{\boldsymbol{A}}\widehat{\boldsymbol{l}}_0^{-1}(\boldsymbol{l} - \boldsymbol{l}_0). \tag{22}$$

where $\widehat{\boldsymbol{E}}$ is an operator that converts vector $\boldsymbol{E}$ into a diagonal matrix.

2.2. Notations of the rigid bodies

2.2.1. Orientation matrix of rigid bodies

Unlike the bars and strings in the rigid body tensegrity, one can use the nodal vector to describe the exact attitude of these axial elements. To describe the attitude of a rigid body, an orientation matrix must be included to show the transition process. There are many approaches to achieve this goal, i.e., Euler angle, Euler principal axis, and quaternion. We chose the Euler angle approach because it is a minimal coordinate method to describe the attitude of rigid bodies. In this problem, we implemented a simple (1–2-3) orientation set, which means to rotate α, β, and γ about the principal axis of $\boldsymbol{b}_1, \boldsymbol{b}_2, \boldsymbol{b}_3$ in sequence in the body-fixed frame. The attitude parameter $\boldsymbol{\varphi}$ is the vector composed of the Euler angle:

$$\boldsymbol{\varphi} = \begin{bmatrix} \alpha \\ \beta \\ \gamma \end{bmatrix}. \tag{23}$$

The attitude matrix is [35]:

$$\begin{aligned} \boldsymbol{R}(\alpha,\beta,\gamma) &= \boldsymbol{R}_3(\gamma)\boldsymbol{R}_2(\beta)\boldsymbol{R}_1(\alpha) \\ &= \begin{bmatrix} \cos\gamma\cos\beta & \cos\gamma\sin\beta\sin\alpha + \sin\gamma\cos\alpha & -\cos\gamma\sin\beta\cos\alpha + \sin\gamma\sin\alpha \\ -\sin\gamma\cos\beta & -\sin\gamma\sin\beta\sin\alpha + \cos\gamma\cos\alpha & \sin\gamma\sin\beta\cos\alpha + \cos\gamma\sin\alpha \\ \sin\beta & -\cos\beta\sin\alpha & \cos\beta\cos\alpha \end{bmatrix}. \end{aligned} \tag{24}$$

Even though the Euler angle has kinematic singularities for the value of $\beta = 0$, this is only a problem in calculating the velocity of orientation parameters from angular velocities. For solving the static equilibrium and form-finding of general tensegrities, there is no such problem using the Euler angle as the orientation parameter.

2.2.2. Mass center of rigid body

Let the mass center of the i th rigid body be $\boldsymbol{n}_{ci} \in \mathbb{R}^{3\times 1}$. Normally, the position of the mass center can be given by measuring the mass distribution of the rigid body in an experiment. However, in the static analysis, the equilibrium of total force and moment is independent of the choice of the mass center. For simplicity, we can directly use the geometry center of the i th rigid body nodes as the mass center:

$$\boldsymbol{n}_{c_i} = \frac{1}{z_i}\boldsymbol{I}_{1,z_i} \bigotimes \boldsymbol{I}_3\boldsymbol{n}_{q_i}, \tag{25}$$

where $\boldsymbol{I}_{1,z_i} \in \mathbb{R}^{1\times z_i}$ is an all-ones vector with z_i columns, and z_i is the number of rigid body nodes in the ith rigid body. Substitute Eq.(12) into Eq. (25), and one can compute the mass center from the nodal coordinate vector of the structure:

$$\boldsymbol{n}_{c_i} = \boldsymbol{E}_{n_{c_i}}^T\boldsymbol{n}, \tag{26}$$

where $\boldsymbol{E}_{n_{c_i}}$ is:

$$\boldsymbol{E}_{n_{ci}} = \frac{1}{z_i}\boldsymbol{E}_{n_{qi}}\boldsymbol{I}_{z_i,1}\otimes\boldsymbol{I}_{3.} \tag{27}$$

2.2.3. Nodal coordinate of rigid bodies

If there is translation or rotation of the rigid bodies, the nodal coordinate of the j th node on the i th rigid body $\boldsymbol{n}_{qij}$ is:

$$\boldsymbol{n}_{qij} = \boldsymbol{n}_{ci} + \boldsymbol{r}_{ij}, \tag{28}$$

$$\boldsymbol{r}_{ij} = \boldsymbol{R}_i^T\left(\boldsymbol{n}_{qij0} - \boldsymbol{n}_{c_{i0}}\right) = \left(\boldsymbol{E}_{n_{ci}}^T - \boldsymbol{E}_{n_{qij}}^T\right)\boldsymbol{n}, \tag{29}$$

where $\boldsymbol{r}_{ij}$ is the vector from the center of mass $\boldsymbol{n}_{ci}$ to the j th node in the i th rigid body, $\boldsymbol{n}_{qij0}$ and $\boldsymbol{n}_{c_{i0}}$ is the nodal coordinate vector of the j th node and the mass center of the i th rigid body in the body-fixed frame. $\boldsymbol{R}_i$ is the attitude matrix of the i th rigid body.

2.3. Minimal coordinate of the system

The minimal coordinate $\boldsymbol{U} \in \mathbb{R}^{n_U}$ is used to represent the position of the free tensegrity nodes and the rigid bodies:

$$\boldsymbol{U} = \begin{bmatrix} \boldsymbol{n}_a \\ \boldsymbol{U}_1 \\ \boldsymbol{U}_2 \\ \vdots \\ \boldsymbol{U}_m \end{bmatrix},$$

where $\boldsymbol{U}_i$ is the minimal coordinate for the i th rigid body, including the position of the mass center $\boldsymbol{n}_{ci} \in \mathbb{R}^3$ and attitude parameter $\boldsymbol{\varphi}_i \in \mathbb{R}^3$:

$$\boldsymbol{U}_i = \begin{bmatrix} \boldsymbol{n}_{c_i} \\ \boldsymbol{\varphi}_i \end{bmatrix}. \tag{31}$$

The location matrix is used to locate minimal coordinate of free tensegrity nodes and rigid bodies:

$$\boldsymbol{U} = \begin{bmatrix} \boldsymbol{E}_{Ua} & \begin{bmatrix} \boldsymbol{E}_{U_{c1}} & \boldsymbol{E}_{U_{\varphi_1}} \end{bmatrix} & \begin{bmatrix} \boldsymbol{E}_{U_{c2}} & \boldsymbol{E}_{U_{\varphi_2}} \end{bmatrix} & \cdots & \begin{bmatrix} \boldsymbol{E}_{U_{cm}} & \boldsymbol{E}_{U_{\varphi m}} \end{bmatrix} \end{bmatrix} \begin{bmatrix} \boldsymbol{n}_a \\ \begin{bmatrix} \boldsymbol{n}_{c1} \\ \boldsymbol{\varphi}_1 \end{bmatrix} \\ \begin{bmatrix} \boldsymbol{n}_{c2} \\ \boldsymbol{\varphi}_2 \end{bmatrix} \\ \vdots \\ \begin{bmatrix} \boldsymbol{n}_{cm} \\ \boldsymbol{\varphi}_m \end{bmatrix} \end{bmatrix}. \tag{32}$$

The nodal coordinate vector of free nodes, mass center, Euler angle, and minimal coordinate of the i th rigid body is:

$$\boldsymbol{n}_a = \boldsymbol{E}_{U_a}^T\boldsymbol{U}, \boldsymbol{n}_{ci} = \boldsymbol{E}_{U_{ci}}^T\boldsymbol{U}, \boldsymbol{\varphi}_i = \boldsymbol{E}_{U_{\varphi_i}}^T\boldsymbol{U}, \boldsymbol{U}_i = \boldsymbol{E}_{U_i}^T\boldsymbol{U}. \tag{33}$$

$\boldsymbol{E}_{U_c}$ and $\boldsymbol{E}_{U_\varphi}$ is used to extract the mass center and Euler angle information of all rigid bodies:

$$\boldsymbol{E}_{Uc} = \begin{bmatrix} \boldsymbol{E}_{Uc1} & \boldsymbol{E}_{Uc2} & \cdots & \boldsymbol{E}_{Ucm} \end{bmatrix}, \boldsymbol{E}_{U\boldsymbol{\varphi}} = \begin{bmatrix} \boldsymbol{E}_{U\boldsymbol{\varphi}_1} & \boldsymbol{E}_{U\boldsymbol{\varphi}_2} & \cdots & \boldsymbol{E}_{U\boldsymbol{\varphi}_m} \end{bmatrix}. \tag{34}$$

$\boldsymbol{E}_{U_i}$ is used to extract the minimal coordinate of the i th rigid body:

$$\boldsymbol{E}_{U_i} = \begin{bmatrix} \boldsymbol{E}_{U_{ci}} & \boldsymbol{E}_{U_{\varphi_i}} \end{bmatrix}. \tag{35}$$

3. Kinematics of the rigid body

3.1. Attitude kinematics

The angular velocity vector of the i th rigid body in the inertial frame is [36]:

$$\boldsymbol{\omega}_i = \begin{bmatrix} \omega_1 \\ \omega_2 \\ \omega_3 \end{bmatrix} = [\boldsymbol{B}_i]\dot{\boldsymbol{\varphi}}_i. \tag{36}$$

The $\boldsymbol{B}_i$ matrix for the Euler angle (1–2-3) orientation set is:

$$\boldsymbol{B}_i = \begin{bmatrix} 1 & 0 & \sin\beta \\ 0 & \cos\alpha & -\cos\beta\sin\alpha \\ 0 & \sin\alpha & \cos\alpha\cos\beta \end{bmatrix}. \tag{37}$$

3.2. Transformation matrix

The velocity vector of the j th node on the i th rigid body is:

$$\dot{\boldsymbol{n}}_{qij} = \dot{\boldsymbol{n}}_{ci} + \boldsymbol{\omega}_i \times \boldsymbol{r}_{ij}. \tag{38}$$

Substitute Eq.(36) into Eq. (38), and we will have:

$$\frac{\mathrm{d}\boldsymbol{n}_{qij}}{\mathrm{d}t} = \frac{\mathrm{d}\boldsymbol{n}_{ci}}{\mathrm{d}t} - \boldsymbol{r}_{ij}^{\times}\boldsymbol{\omega}_i = \frac{\mathrm{d}\boldsymbol{n}_{ci}}{\mathrm{d}t} - \boldsymbol{r}_{ij}^{\times}\boldsymbol{B}_i\frac{\mathrm{d}\boldsymbol{\varphi}_i}{\mathrm{d}t}. \tag{39}$$

where $\boldsymbol{r}_{ij}^{\times}$ is the anti-symmetric matrix of the vector $\boldsymbol{r}_{ij}$. Eliminate the time derivative part, and the above equation can be written as:

$$\mathrm{d}\boldsymbol{n}_{qij} = \mathrm{d}\boldsymbol{n}_{ci} - \boldsymbol{r}_{ij}^{\times}\boldsymbol{B}_i\mathrm{d}\boldsymbol{\varphi}_i. \tag{40}$$

So, the partial derivative of $\boldsymbol{n}_{q_{ij}}$ to $\boldsymbol{U}_i$ is:

$$\overline{\boldsymbol{G}}_{ij} = \frac{\partial\boldsymbol{n}_{qij}}{\partial\boldsymbol{U}_i^T} = [\boldsymbol{I}_3 \quad -\boldsymbol{r}_{ij}^{\times}\boldsymbol{B}_i], \tag{41}$$

where $\frac{\partial\boldsymbol{a}}{\partial\boldsymbol{b}^T}$ and $\frac{\partial\boldsymbol{b}^T}{\partial\boldsymbol{a}}$ represent the partial derivative of vector $\boldsymbol{a}$ to vector $\boldsymbol{b}$ in numerator layout, respectively. The partial derivative of $\boldsymbol{n}_{q_{ij}}$ to the minimal coordinate $\boldsymbol{U}$ is:

$$\boldsymbol{G}_{ij} = \frac{\partial\boldsymbol{n}_{qij}}{\partial\boldsymbol{U}^T} = \frac{\partial\boldsymbol{n}_{qij}}{\partial\boldsymbol{U}_i^T}\frac{\partial\boldsymbol{U}_i}{\partial\boldsymbol{U}^T} = \overline{\boldsymbol{G}}_{ij}\boldsymbol{E}_{U_i}^T. \tag{42}$$

The transformation matrix $\boldsymbol{G}$ of the entire structure is:

$$\boldsymbol{G} = \frac{\partial\boldsymbol{n}}{\partial\boldsymbol{U}^T} = \frac{\partial\left(\boldsymbol{E}_{n_a}\boldsymbol{n}_a + \sum_{i=1}^{m}\sum_{j=1}^{z_i}\boldsymbol{E}_{n_{qij}}\boldsymbol{n}_{qij}\right)}{\partial\boldsymbol{U}^{\mathrm{T}}} = \boldsymbol{E}_{n_a}\boldsymbol{E}_{U_a}^T + \sum_{i=1}^{m}\sum_{j=1}^{z_i}\boldsymbol{E}_{n_{qij}}\boldsymbol{G}_{ij}, \tag{43}$$

which maps the difference of nodal coordinate $\boldsymbol{n}$ to the difference of minimal coordinate $\boldsymbol{U}$.

4. Equilibrium equation

4.1. The Lagrangian method

The general form of the Lagrangian equation is:

$$\frac{\mathrm{d}}{\mathrm{d}t}\frac{\partial L}{\partial\dot{\boldsymbol{U}}} - \frac{\partial L}{\partial\boldsymbol{U}} = \boldsymbol{Q}_{np}, \tag{44}$$

where $L = T - V$ is the Lagrangian function, T and V are the kinetic energy and potential energy of the system, $\boldsymbol{Q}_{np}$ is the non-potential force vector of the general tensegrity structures, $\boldsymbol{U}$ is the minimal coordinate of the system. For the statics problem, the kinetic energy T is zero in this study, and we study the potential energy of the system. For statics problems, the Lagrangian method degenerates to:

$$\frac{\partial V}{\partial\boldsymbol{U}} = \boldsymbol{Q}_{np}. \tag{45}$$

Note that Eq.(45) is consistent with the principle of stationary total potential energy and the principle of virtual work. However, using the Lagrangian method to derive the equilibrium equation will make it easy to extend to the future study of the dynamic problem. It is required in the Lagrangian method to use minimal coordinate as the variable, which is

critical for the derivation. Note that if we use variables with over-parameterization like the Euler parameter, modified Rodrigues parameters, etc., there will be an issue in violation of the constraints of the variables.

4.2. Energy function

The total potential energy V of the tensegrity system with the rigid body is composed of strain potential energy V_e and gravitational potential energy V_g:

$$V = V_e + V_g. \tag{46}$$

4.2.1. Strain potential energy

There is no deformation in a rigid body, so the strain potential energy for a rigid body is zero. The strain potential energy is only stored in the axial members:

$$V_e = \sum\nolimits_{i=1}^{n_e} \int_{l_{0_i}}^{l_i} t_i \mathrm{d}x. \tag{47}$$

From the statics equation of traditional tensegrity [37], we can compute the partial derivative of V_e to $\boldsymbol{U}$, $\frac{\partial V_e}{\partial \boldsymbol{n}}$:

$$\frac{\partial V_e}{\partial \boldsymbol{U}} = \frac{\partial \boldsymbol{n}^T}{\partial \boldsymbol{U}} \frac{\partial V_e}{\partial \boldsymbol{n}} = \boldsymbol{G}^T \left(\boldsymbol{C}^T \widehat{\boldsymbol{l}}^{-1} \widehat{\boldsymbol{t}} \boldsymbol{C}\right) \otimes \boldsymbol{I}_3 \boldsymbol{n}. \tag{48}$$

4.2.2. Gravitational potential energy

The gravitational potential energy is relative to any member that has mass. In tensegrity with a rigid body, all axial members, point mass, and rigid body will contribute to gravitational potential energy:

$$V_g = V_{ge} + V_{gp} + V_{gr}. \tag{49}$$

The gravitational potential energy corresponding to the axial elements V_{ge} is:

$$V_{ge} = \sum_{i=1}^{n^e} \frac{m_{ei}}{2} [a_x \quad a_y \quad a_z] \begin{bmatrix} x_j^i + x_k^i \\ y_j^i + y_k^i \\ z_j^i + z_k^i \end{bmatrix} = \sum_{i=1}^{n_e} \frac{m_{ei}}{2} [a_x \quad a_y \quad a_z] |C_i| \otimes I_3 n$$

$$= \frac{1}{2} \left(m_e^T |C|\right) \otimes [a_x \quad a_y \quad a_z] n, \tag{50}$$

where m_{ei} is the mass of the ith axial element, and $\boldsymbol{m}_e$ is the mass vector of all axial elements.a_x, a_y, a_z are the gravitational acceleration in the X, Y, and Z-axis, respectively. The gravitational potential energy corresponding to point mass V_{gp} is:

$$V_{gp} = \sum\nolimits_{i=1}^{n_n} m_{pi} \otimes [a_x \quad a_y \quad a_z] \begin{bmatrix} x_i \\ y_i \\ z_i \end{bmatrix} = \boldsymbol{m}_p^T \otimes [a_x \quad a_y \quad a_z] \boldsymbol{n} \tag{51}$$

where m_{pi} is the mass of the ith node, and $\boldsymbol{m}_p$ is the node mass vector. The gravitational potential energy corresponding to the rigid body V_{gr} is:

$$\begin{aligned} V_{gr} &= \sum\nolimits_{i=1}^{n_q} m_{qi} \otimes [a_x \quad a_y \quad a_z] \boldsymbol{n}_{ci} \\ &= \boldsymbol{m}_q^T \otimes [a_x \quad a_y \quad a_z] \begin{bmatrix} \boldsymbol{n}_{c1} \\ \vdots \\ \boldsymbol{n}_{cm} \end{bmatrix} \\ &= \boldsymbol{m}_q^T \otimes [a_x \quad a_y \quad a_z] \boldsymbol{E}_{U_c}^T \boldsymbol{U} \end{aligned} \tag{52}$$

where m_{qi} is the mass of the ith rigid body, and $\boldsymbol{m}_q$ is the mass vector rigid bodies. The partial derivative of V_g to $\boldsymbol{n}$ is:

$$\begin{aligned} \frac{\partial V_g}{\partial \boldsymbol{U}} &= \frac{\partial \boldsymbol{n}^T}{\partial \boldsymbol{U}} \left(\frac{\partial V_{ge}}{\partial \boldsymbol{n}} + \frac{\partial V_{gm}}{\partial \boldsymbol{n}}\right) + \frac{\partial V_{gr}}{\partial \boldsymbol{U}} \\ &= \left\{ \boldsymbol{G}^T \left(\frac{1}{2} |\boldsymbol{C}|^T \boldsymbol{m}_e + \boldsymbol{m}_p \right) + \boldsymbol{E}_{U_c} \boldsymbol{m}_q \right\} \otimes [a_x \quad a_y \quad a_z]^T = \boldsymbol{g}, \end{aligned} \tag{53}$$

where $\boldsymbol{g}$ is the gravitational force vector.

4.3. Nonlinear equilibrium equation

The statics equation of tensegrity with the rigid body is calculated by the partial derivative of V with respect to $\boldsymbol{U}$:

$$\frac{\partial V}{\partial \boldsymbol{U}} = \frac{\partial V_e}{\partial \boldsymbol{U}} + \frac{\partial V_g}{\partial \boldsymbol{U}} = \boldsymbol{Q}_{np}. \tag{54}$$

Substitute the Eq.(48) and Eq.(53) into Eq.(54), and we will have:

$$\boldsymbol{G}^T \left(\boldsymbol{C}^T \widehat{\boldsymbol{l}}^{-1} \widehat{\boldsymbol{t}} \boldsymbol{C}\right) \otimes \boldsymbol{I}_3 \boldsymbol{n} = \boldsymbol{Q}_{np} - \boldsymbol{g}. \tag{55}$$

Eq.(55) is the static equilibrium equation of the general tensegrity system with rigid bodies. The second part $\left(\boldsymbol{C}^T \widehat{\boldsymbol{l}}^{-1} \widehat{\boldsymbol{t}} \boldsymbol{C}\right) \otimes \boldsymbol{I}_3 \boldsymbol{n}$ is the collection of inner force of members in nodes, which is identical to $\boldsymbol{Kn}$ in traditional tensegrity structure [37]. Note that $\left(\boldsymbol{C}^T \widehat{\boldsymbol{l}}^{-1} \widehat{\boldsymbol{t}} \boldsymbol{C}\right) \otimes \boldsymbol{I}_3$ is a nonlinear function of nodal coordinate, so Eq. (55) is nonlinear. The first part $\boldsymbol{G}^T$ transforms the nodal force from the node space to body space, which is identity to the generalized force. Eq.(55) can be written into a simple form:

$$\boldsymbol{K}_r \boldsymbol{n} = \boldsymbol{Q}_{np} - \boldsymbol{g}, \tag{56}$$

where $\boldsymbol{K}_r$ is the stiffness matrix of general tensegrity with nodal coordinate vector $\boldsymbol{n}$ as the variable:

$$\boldsymbol{K}_r = \boldsymbol{G}^T \left(\boldsymbol{C}^T \widehat{\boldsymbol{l}}^{-1} \widehat{\boldsymbol{t}} \boldsymbol{C}\right) \otimes \boldsymbol{I}_3. \tag{57}$$

The right part of Eq. (54) is the generalized force $\boldsymbol{Q}_{np}$, which can be calculated by using the transformation matrix [35]:

$$\begin{aligned} \boldsymbol{Q}_{np} &= \frac{\partial \boldsymbol{n}^T}{\partial \boldsymbol{U}} \boldsymbol{f} + \sum\nolimits_{i=1}^{n_e} \frac{\partial \boldsymbol{n}_{ci}^T}{\partial \boldsymbol{U}} \boldsymbol{f}_{ci} + \sum\nolimits_{i=1}^{n_e} \frac{\partial \boldsymbol{\omega}_i^T}{\partial \dot{\boldsymbol{U}}} \boldsymbol{m}_{ci} \\ &= \boldsymbol{G}^T \boldsymbol{f} + \sum\nolimits_{i=1}^{n_e} \boldsymbol{E}_{Uci} \boldsymbol{f}_{ci} + \sum\nolimits_{i=1}^{n_e} \boldsymbol{E}_{U\varphi i} \boldsymbol{B}_i^T \boldsymbol{m}_{ci} = \boldsymbol{G}^T \boldsymbol{f} + \boldsymbol{E}_{U_c} \boldsymbol{f}_c + \boldsymbol{E}_{U_\varphi} \boldsymbol{B}^T \boldsymbol{m}_c, \end{aligned} \tag{58}$$

where $\boldsymbol{f}$ is the non-potential external force vector exerted on the tensegrity node. $\boldsymbol{f}_{ci}$ and $\boldsymbol{m}_{ci}$ is the total force and moment exerted on the i th rigid body. $\boldsymbol{f}_c$ and $\boldsymbol{m}_c$ are the collection of force and moment of all rigid bodies.

$$\boldsymbol{f}_c = \begin{bmatrix} \boldsymbol{f}_{c1} \\ \vdots \\ \boldsymbol{f}_{cm} \end{bmatrix}, \boldsymbol{m}_c = \begin{bmatrix} \boldsymbol{m}_{c1} \\ \vdots \\ \boldsymbol{m}_{cm} \end{bmatrix}. \tag{59}$$

$\boldsymbol{B}$ matrix is defined as:

$$\boldsymbol{B} = \begin{bmatrix} \boldsymbol{B}_1 \\ \ddots \\ \boldsymbol{B}_m \end{bmatrix}. \tag{60}$$

4.4. Linearized equilibrium equation

4.4.1. Linearized equilibrium equation with minimal coordinate as the variable

Using Taylor's expansion of Eq. (56) about a configuration $\boldsymbol{n}^i$ in the ith iteration step, we have the linearized equilibrium equation:

$$\boldsymbol{K}_r|_{\boldsymbol{n}^i} \boldsymbol{n}^i + \boldsymbol{K}_{Tr} \left(\boldsymbol{U}^{i+1} - \boldsymbol{U}^i\right) = \boldsymbol{Q}_{np} - \boldsymbol{g}, \tag{61}$$

where $\boldsymbol{K}_{Tr}$ is the tangent stiffness matrix of the structure, $\boldsymbol{U}^i$ is the

minimal coordinate corresponding to $\boldsymbol{n}^i$. $\mathbf{K_r}|_{\mathbf{n}^i}$ is the stiffness matrix in $\boldsymbol{n}^i$ configuration. By solving Eq.(61), we can obtain a new configuration $\boldsymbol{U}^{i+1}$ in the $i+1$ iteration step, which is closer to the equilibrium configuration. The out-of-balance forces of the system are defined as:

$$\boldsymbol{P}^i = \boldsymbol{Q}_{np} - \boldsymbol{g} - \boldsymbol{K}_r|_{\boldsymbol{n}^i}\boldsymbol{n}^i. \tag{62}$$

The difference of the minimal coordinate can be simply computed by:

$$\mathrm{d}\boldsymbol{U}^i = \boldsymbol{K}_{Tr}^{-1}\boldsymbol{P}^i. \tag{63}$$

The above three equations can be used in solving nonlinear equilibrium equations based on an iteration method.

4.4.2. Linearized equilibrium equation in terms of the member force

Eq.(55) can be written linearly in terms of the member force $\boldsymbol{t}$:

$$\boldsymbol{A}_r\boldsymbol{t} = \boldsymbol{Q}_{np} - \boldsymbol{g}, \tag{64}$$

where $\boldsymbol{A}_r \in \mathbb{R}^{n_U \times n_e}$ is the equilibrium matrix for tensegrity with rigid bodies:

$$\boldsymbol{A}_r = \boldsymbol{G}^T\boldsymbol{A}_2. \tag{65}$$

where $\boldsymbol{A}_2$ is the equilibrium equation of traditional tensegrity [37]:

$$\boldsymbol{A}_2 = \boldsymbol{C}^T \otimes \boldsymbol{I}_3 \mathrm{b.d.}(\boldsymbol{H})\widehat{\boldsymbol{l}}^{-1}, \tag{66}$$

where $\mathrm{b.d.}(\boldsymbol{H})$ is the block diagonal matrix of $\boldsymbol{H}$. Note that the equilibrium matrix for tensegrity with rigid bodies $\boldsymbol{A}_r$ is identical to the $\boldsymbol{C}$ matrix in Wang et al. [28]. The singular value decomposition of the equilibrium matrix $\boldsymbol{A}_r$ reveals the self-stress mode and mechanism mode of the structure [38]:

$$\boldsymbol{A}_r = \boldsymbol{W}\Sigma\boldsymbol{V}^T = [\,\boldsymbol{W}_1 \quad \boldsymbol{W}_2\,]\begin{bmatrix}\Sigma_0 & 0\\ 0 & 0\end{bmatrix}\begin{bmatrix}\boldsymbol{V}_1^T\\ \boldsymbol{V}_2^T\end{bmatrix}, \tag{67}$$

where $\boldsymbol{W} \in \boldsymbol{R}^{n_U \times n_U}$, and $\boldsymbol{V} \in \boldsymbol{R}^{n_e \times n_e}$ are orthogonal matrices. Let $r = \mathrm{rank}(\boldsymbol{A}_r)$ be the rank of $\boldsymbol{A}_r$. $\boldsymbol{V}_1 \in \boldsymbol{R}^{n_e \times r}, \boldsymbol{V}_2 \in \boldsymbol{R}^{n_e \times (n_e - r)}$ is respectively the row space and null space of $\boldsymbol{A}_r$, and $\boldsymbol{W}_1 \in \boldsymbol{R}^{n_U \times r}, \boldsymbol{W}_2 \in \boldsymbol{R}^{n_U \times (n_U - r)}$ is respectively the column space and left null space of $\boldsymbol{A}_r$. $\boldsymbol{A}_r\boldsymbol{V}_2 = 0$ and $\boldsymbol{A}_r^T\boldsymbol{W}_2 = 0$, $\boldsymbol{V}_2$ and $\boldsymbol{W}_2$ are the self-stress mode and mechanism mode of the tensegrity structure, respectively.

4.4.3. Compatibility equation

The compatibility equation is the relation between $\mathrm{d}\boldsymbol{U}$ and $\mathrm{d}\boldsymbol{l}$ that guarantees the structural deformations are physically valid. The compatibility equation of the structure is:

$$\boldsymbol{B}_r\mathrm{d}\boldsymbol{U} = \mathrm{d}\boldsymbol{l}, \tag{68}$$

where $\boldsymbol{B}_r \in \mathbb{R}^{n_e \times n_U}$ is the compatibility matrix:

$$\boldsymbol{B}_r = \frac{\partial \boldsymbol{l}}{\partial \boldsymbol{U}^T} = \frac{\partial \boldsymbol{l}}{\partial \boldsymbol{n}^T}\frac{\partial \boldsymbol{n}}{\partial \boldsymbol{U}^T} = \boldsymbol{A}_2^T\boldsymbol{G}. \tag{69}$$

It can be found that the compatibility matrix is the transpose of the equilibrium matrix:

$$\boldsymbol{B}_r = \boldsymbol{A}_r^T. \tag{70}$$

This can also be proved by the principle of virtual work.

4.5. Tangent stiffness matrix

Refer to the derivation of tangent stiffness in Chen and Jiang [29], the tangent stiffness matrix of the general tensegrity with a rigid body is:

$$\boldsymbol{K}_{Tr} = \frac{\partial\left(\boldsymbol{B}_r^T\boldsymbol{t}\right)}{\partial \boldsymbol{U}^T} = \boldsymbol{B}_r^T\frac{\partial \boldsymbol{t}}{\partial \boldsymbol{U}^T} + \frac{\partial \boldsymbol{B}_r^T}{\partial \boldsymbol{U}^T}\boldsymbol{t} = \boldsymbol{K}_E + \boldsymbol{K}_G. \tag{71}$$

The first part of Eq.(71) is the material stiffness $\boldsymbol{K}_E$ caused by the difference of member force:

$$\boldsymbol{K}_E = \boldsymbol{B}_r^T\frac{\partial \boldsymbol{t}}{\partial \boldsymbol{l}^T}\frac{\partial \boldsymbol{l}}{\partial \boldsymbol{U}^T} = \boldsymbol{B}_r^T\widehat{\boldsymbol{k}}\boldsymbol{B}_r = \boldsymbol{A}_r\widehat{\boldsymbol{k}}\boldsymbol{A}_r^T, \tag{72}$$

where $\boldsymbol{k} = \widehat{\boldsymbol{E}}\widehat{\boldsymbol{A}}\boldsymbol{l}_0^{-1}$ is the stiffness of the axial members. The second part of Eq.(71) is the geometry stiffness $\boldsymbol{K}_G$ caused by the difference of structural shape:

$$\boldsymbol{K}_G = \frac{\partial \boldsymbol{B}_r^T}{\partial \boldsymbol{U}^T}\boldsymbol{t} = \boldsymbol{\Omega}^T\boldsymbol{t} = \sum\nolimits_{i=1}^{n_s}\boldsymbol{\Omega}_i^T\boldsymbol{t}_i, \tag{73}$$

where the Hessian matrix $\boldsymbol{\Omega} \in \mathbb{R}^{n_e \times n_U \times n_U}$ is expressed as:

$$\boldsymbol{\Omega} = \frac{\partial \boldsymbol{B}_r}{\partial \boldsymbol{U}} = \left[\,\boldsymbol{\Omega}_1^T \quad \cdots \quad \boldsymbol{\Omega}_i^T \quad \cdots \quad \boldsymbol{\Omega}_{n_e}^T\,\right]^T, \tag{74}$$

where $\Omega_i = \frac{\partial \boldsymbol{B}_{ri}}{\partial \boldsymbol{U}} \in \mathbb{R}^{n_U \times n_U}$ is the i th member's Hessian matrix, and $\boldsymbol{B}_{ri}$ is the ith row of $\boldsymbol{B}_r$. Note that the explicit formulation of $\boldsymbol{\Omega}$ is vital to calculate the geometry stiffness matrix. Fortunately, $\boldsymbol{\Omega}_i$ can be obtained by calculating and comparing two equivalent expressions of the ith cable's acceleration $\ddot{\boldsymbol{l}}_i$. Eq. (78) is equivalent to:

$$\dot{\boldsymbol{l}}_i = \boldsymbol{B}_{ri}\dot{\boldsymbol{U}}. \tag{75}$$

Using $\frac{\partial \boldsymbol{B}_{ri}}{\partial t} = \frac{\partial \boldsymbol{U}^T}{\partial t}\frac{\partial \boldsymbol{B}_{ri}}{\partial \boldsymbol{U}} = \dot{\boldsymbol{U}}^T\boldsymbol{\Omega}_i$, the i th cable's acceleration $\ddot{\boldsymbol{l}}_i$ is:

$$\ddot{\boldsymbol{l}}_i = \boldsymbol{B}_{ri}\ddot{\boldsymbol{U}} + \frac{\partial \boldsymbol{B}_{ri}}{\partial \boldsymbol{t}}\dot{\boldsymbol{U}} = \boldsymbol{B}_{ri}\ddot{\boldsymbol{U}} + \dot{\boldsymbol{U}}^T\boldsymbol{\Omega}_i\dot{\boldsymbol{U}}. \tag{76}$$

From the derivation in Appendix, the ith cable's acceleration $\ddot{\boldsymbol{l}}_i$ is expressed as:

$$\ddot{\boldsymbol{l}}_i = \boldsymbol{B}_{ri}\ddot{\boldsymbol{U}} + \dot{\boldsymbol{U}}^T\left(\boldsymbol{G}^T\left(\boldsymbol{C}_i^T \otimes \boldsymbol{I}_3\right)\frac{\boldsymbol{P}_{hn_i}}{l_i}(\boldsymbol{C}_i \otimes \boldsymbol{I}_3)\boldsymbol{G} + \boldsymbol{F}_i\right)\dot{\boldsymbol{U}}. \tag{77}$$

Comparing Eq. (76) with Eq. (77), the matrix $\boldsymbol{\Omega}_i$ is written as:

$$\boldsymbol{\Omega}_i = \boldsymbol{G}^T\left(\boldsymbol{C}_i^T \otimes \boldsymbol{I}_3\right)\frac{\boldsymbol{P}_{hn_i}}{l_i}(\boldsymbol{C}_i \otimes \boldsymbol{I}_3)\boldsymbol{G} + \boldsymbol{F}_i, \tag{78}$$

where $\boldsymbol{P}_{hn_i} = \boldsymbol{I}_3 - \boldsymbol{h}_{n_i}\boldsymbol{h}_{n_i}^T \in \mathbb{R}^{3\times 3}$ denotes the projector to the plane with the normal vector $\boldsymbol{h}_{n_i}$, in which $\boldsymbol{h}_{n_i} = \frac{\boldsymbol{h}_i}{l_i}$ is the ith cable's unit vector. From the derivation in Appendix, the matrix $\boldsymbol{F}_i \in \mathbb{R}^{n_U \times n_U}$ is written as:

$$\boldsymbol{F}_i = \sum\nolimits_{j=1}^{m}\sum\nolimits_{k=1}^{z_i}\boldsymbol{E}_{Uj}\begin{bmatrix}0 & 0\\ 0 & \boldsymbol{B}_j^T\boldsymbol{z}_{ijk}^{\times}\boldsymbol{r}_{jk}^{\times}\boldsymbol{B}_j\end{bmatrix}\boldsymbol{E}_{Uj}^T, \tag{79}$$

in which $\boldsymbol{z}_{ijk} \in \mathbb{R}^3$ is:

$$\boldsymbol{z}_{ijk} = \left(\boldsymbol{h}_{n_i}^T(\boldsymbol{C}_i \otimes \boldsymbol{I}_3)\boldsymbol{E}_{n_{ijk}}\right)^T. \tag{80}$$

Note that the tangent stiffness is a general form of classical tensegrity. If there is no rigid body, the tangent stiffness will degenerate to a classical tensegrity [37]. Also, note that the above derivation is generally consistent with the formulation in Chen and Jiang [29]. The difference is that the proposed formulation in this paper can consider free and pinned tensegrity nodes in the general tensegrity system, and the use of the location matrix makes the formulation in Eq.(79) be expressed in a more neat and straightforward form.

5. Form-finding of tensegrity systems with rigid bodies

In this section, we formulate the form-finding method for tensegrity systems with rigid bodies. Three numerical examples are carried out to illustrate the accuracy and efficiency of the proposed form-finding method.

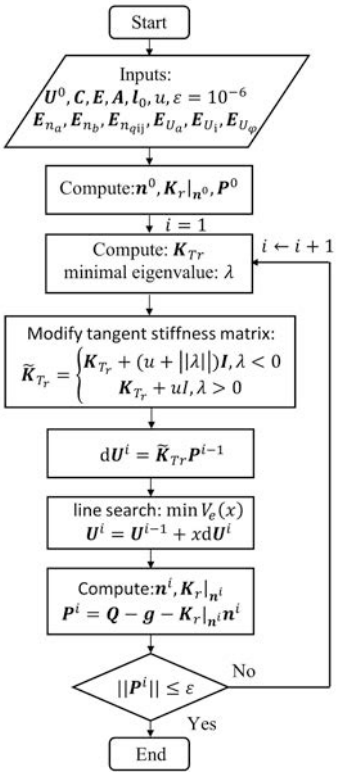

Fig. 2. Flow chart of the form-finding algorithm.

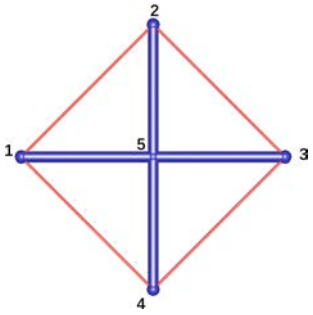

Fig. 3. The initial configuration of a T-bar.

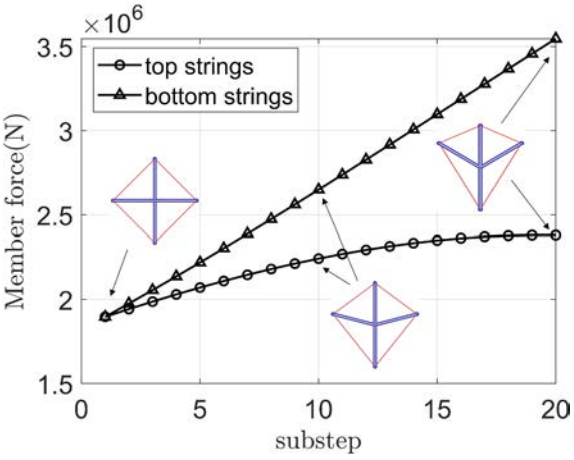

Fig. 4. The member forces in each substep.

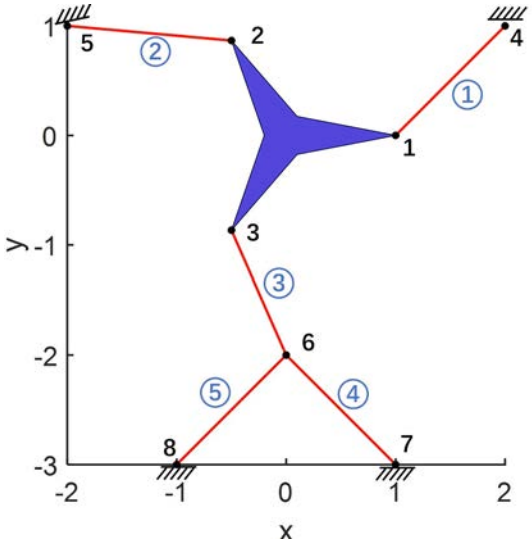

Fig. 5. The initial configuration.

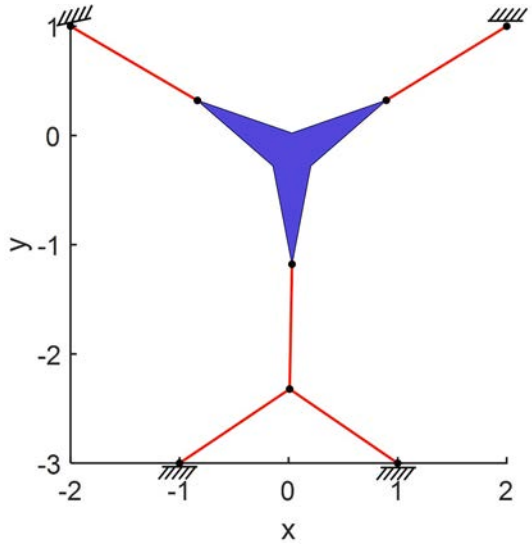

Fig. 6. The equilibrium configuration.

5.1. Form-finding method

5.1.1. Form-finding procedure

The form-finding method is basically solving the nonlinear equilibrium equation. However, the self-equilibrated tensegrities lacking proper constraints have several problems in solving its equilibrium equation [39]. Firstly, the rigid body mode will lead to a singular tangent stiffness matrix. Newton's method is not able to solve the equation with a singular Hessian matrix. Secondly, the tangent stiffness matrix may have a negative eigenvalue, and the result of solving the nonlinear equilibrium equation will converge to an unstable equilibrium configuration. To ensure the result is stable equilibrium, modifying the tangent stiffness matrix to positive definite is necessary. Thirdly, an appropriate optimization objective must be defined to guarantee that the result approaches the equilibrium configuration. The form-finding procedure consists of the following main steps, as shown in Fig. 2.

Inputs:

(1) Specify the primary data of a tensegrity system with rigid bodies, including the minimal coordinate $\boldsymbol{U}_0$, connectivity matrix $\boldsymbol{C}$, axial stiffnesses vector $\boldsymbol{E}$, cross-section area vector $\boldsymbol{A}$, rest length vector $\boldsymbol{l}_0$, location matrix $\boldsymbol{E}_{n_a}, \boldsymbol{E}_{n_b}, \boldsymbol{E}_{n_{qij}}, \boldsymbol{E}_{U_a}, \boldsymbol{E}_{U_i}, \boldsymbol{E}_{U_\varphi}$, coefficient u and ε. Compute

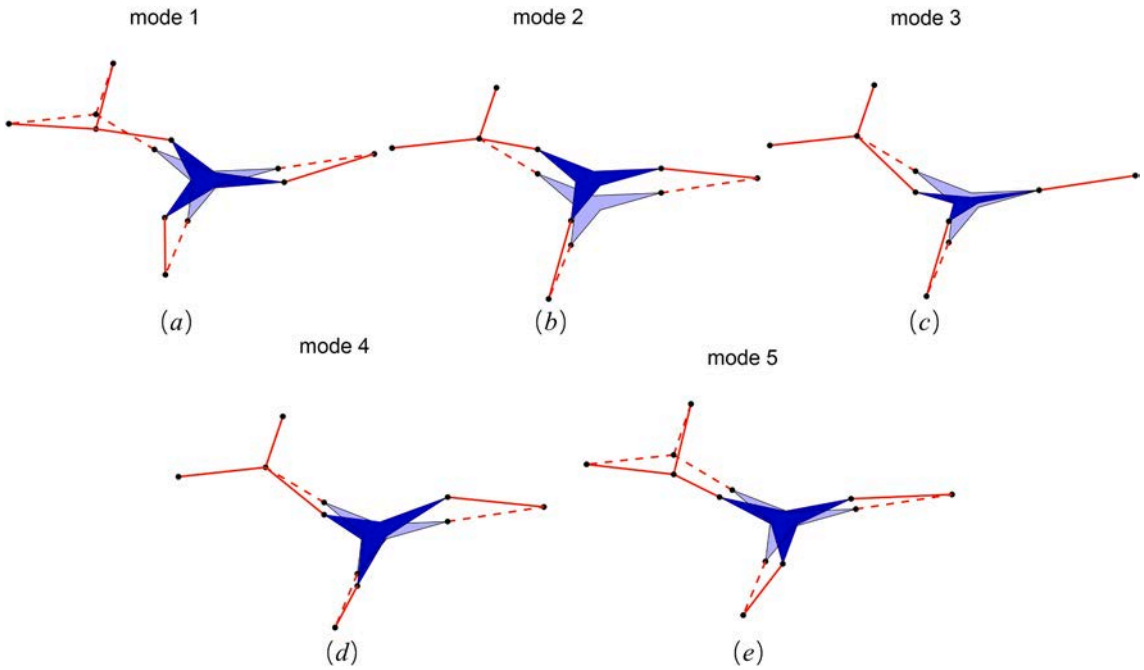

Fig. 7. The five mechanism modes of the structure.

Fig. 8. Eigenvalue of the tangent stiffness matrix.

the nodal coordinate $\boldsymbol{n}^0$, stiffness matrix $K_r|n^0$, out-of-balance force $\boldsymbol{P}^0$ in the initial configuration.

Iteration:

(2) Compute the tangent stiffness $\boldsymbol{K}_{Tr}$ for the structure in the current configuration. Compute the minimal eigenvalue of the $\boldsymbol{K}_{Tr}$ as λ.

(3) Check whether the tangent stiffness matrix is positive definite or not. Use the method in Section 5.1.2 to modify the stiffness matrix such that it is positive definite.

(4) Solve the difference of minimal coordinate $\mathrm{d}\boldsymbol{U}^i$, employ the line search algorithm in Section 5.1.3 to calculate the updated minimal coordinate $\boldsymbol{U}^i$.

(5) Calculate the nodal coordinate $\boldsymbol{n}^i$, stiffness matrix $\boldsymbol{K}_r\boldsymbol{n}^i$ and out-of-balance forces $\boldsymbol{P}^i$. Check whether the current configuration is in equilibrium or not. If not, set $i \leftarrow i+1$ and go to step (2).

(6) Terminate the iteration when an equilibrium configuration has been obtained.

5.1.2. *Modification of tangent stiffness matrix*

To guarantee the form-finding result converges to a stable equilibrium. The positive definiteness of the tangent stiffness matrix $\boldsymbol{K}_{Tr}$ should be examined and modified. For the configuration $\boldsymbol{U}_i$ at an iteration step, if the minimal eigenvalue of the tangent stiffness matrix λ is negative, a sufficiently large identity matrix $(|\lambda| + u)\boldsymbol{I}$ will be added to $\boldsymbol{K}_{Tr}$ to obtain the modified tangent stiffness matrix $\widetilde{\boldsymbol{K}}_{Tr}$, where u is a positive coefficient to guarantee the modified tangent stiffness matrix is not seriously ill. Otherwise, $u\boldsymbol{I}$ will be added to the tangent stiffness matrix:

$$\widetilde{\boldsymbol{K}}_{T_r} = \begin{cases} \boldsymbol{K}_{T_r} + (u + \|\lambda\|)\boldsymbol{I}, \lambda < 0 \\ \boldsymbol{K}_{T_r} + u\boldsymbol{I}, \lambda > 0 \end{cases}. \tag{81}$$

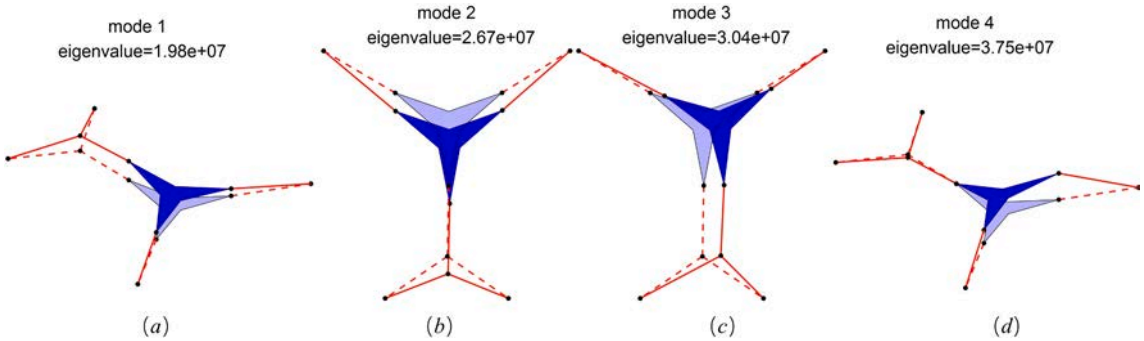

Fig. 9. Deformed shapes of the modes corresponding to the first four eigenvalues.

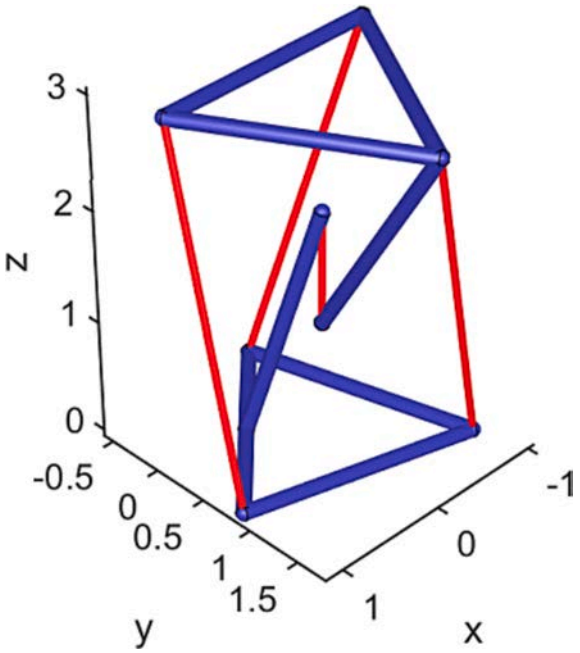

Fig. 10. The initial configuration of the tensegrity table.

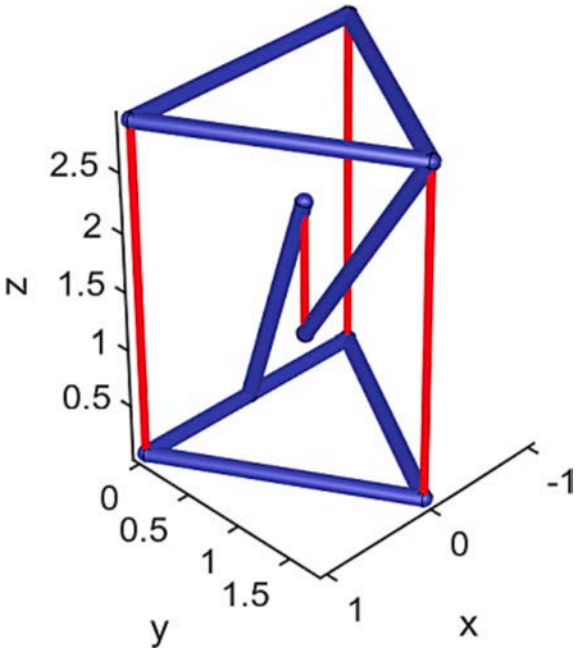

Fig. 11. The equilibrium configuration of the tensegrity table.

From experience, in this paper, we set $u = 0.1$. Using the modified tangent stiffness matrix, the increment of the generalized coordinate vector $\mathrm{d}\boldsymbol{U}$ can be obtained from Eq. (63):

$$\mathrm{d}\boldsymbol{U}^i = \widetilde{\boldsymbol{K}}_{Tr}^{-1}\boldsymbol{P}^i. \tag{82}$$

5.1.3. Line search algorithm

To increase the convergence speed of solving the nonlinear equilibrium equation. We use a line search algorithm [39,40] in each iteration step to minimize the total potential energy of the system. In the ith step, we update the minimal coordinate vector $\boldsymbol{U}_i$ from that in step $i-1$ by:

$$\boldsymbol{U}_i = \boldsymbol{U}_{i-1} + x\mathrm{d}\boldsymbol{U}^i, \tag{83}$$

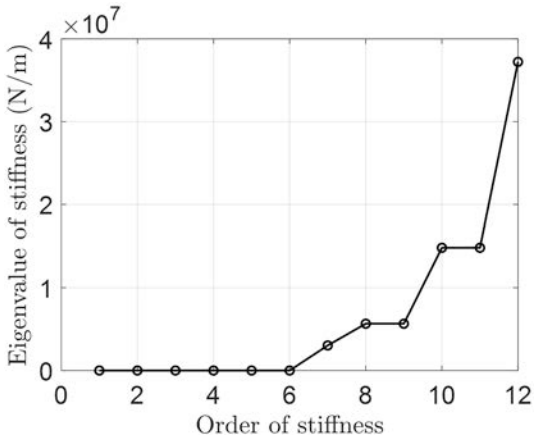

Fig. 12. Eigenvalues of the tangent stiffness matrix.

where the coefficient x is determined by the following optimization problem of single-variable function on the fixed interval:

$$\begin{aligned} &\min V(x) \\ &\text{s.t.} 0 < x \leq 1. \end{aligned} \tag{84}$$

Given $\boldsymbol{U}_i$, the nodal coordinate vector $\boldsymbol{n}_i$ can be calculated by Eqs.(9), (24), and (28). And the total potential energy can be calculated by Eqs. (46) to (2). The line search algorithm can be simply implemented by the 'fminbnd' function in MATLAB.

5.2. Numerical examples

In this section, four examples are studied to demonstrate the accuracy and efficiency of the proposed form-finding method for tensegrity with rigid bodies. Different examples are chosen to represent generalized tensegrity with none, one, or multiple rigid bodies, with or without free and pinned nodes. In these examples, the equilibrium configurations and prestress are tuned by varying the rest length of the strings in the structure. The tangent modulus and cross-sectional area of the strings in all the examples are set to be 7.6×10^{10}Pa and 1×10^{-4}m^2.

5.2.1. T-bar unit

In this example, we would like to show that the system degrades to a traditional tensegrity structure without arbitrary rigid bodies. A T-Bar unit consisting of four bars and four strings has been proven to be a mass efficient structure in taking compressive loads [34]. Tran and Lee have shown the T-Bar example regarding the form-finding research [41]. Using the same configuration described in [41], as shown in Fig. 3, we assign non-equilibrium to prestress in the structure and check the deformed configuration. The rest length of bars and the two bottom strings are set to be $\boldsymbol{l}$ and $0.8\boldsymbol{l}$, the rest length of the two top strings is decreased from $0.8\boldsymbol{l}$ to $0.5\boldsymbol{l}$ equally in each substep, where $\boldsymbol{l}$ is the present length of members in the initial configuration. The equilibrium configuration and member force are obtained by the form-finding method, and the results are shown in Fig. 4.

5.2.2. Patio shade cover

This example presents a structure composed of a rigid triangle piece, five strings, a free node, and four pinned nodes. The index of nodes and elements are marked in black numbers and blue numbers in circles, respectively, as shown in Fig. 5. And Fig. 5 is the initial configuration of the generalized tensegrity. To generate the prestress of the structure, the rest length of strings is set to be 0.3 times the present length in the initial configuration, which is $\boldsymbol{l}_0 = 0.3\boldsymbol{l}$. Fig. 6 gives the equilibrium configuration of the form-finding result.

The nodal coordinate matrix $\boldsymbol{N} \in \mathbb{R}^{3\times 8}$ in the equilibrium configuration in the form of Eq. (3) is given as:

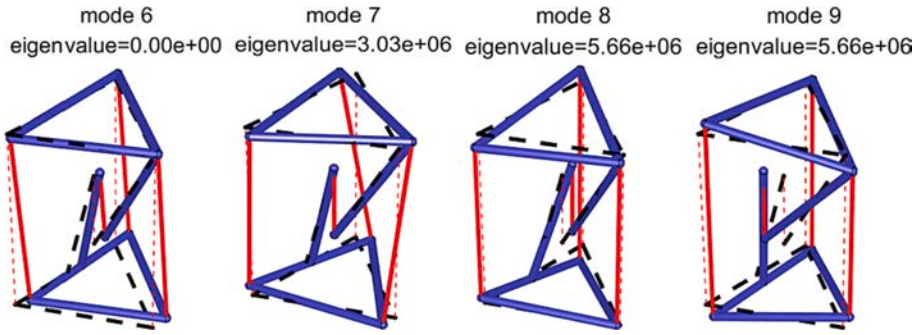

Fig. 13. The mode shapes and the eigenvalues of the tangent stiffness matrix.

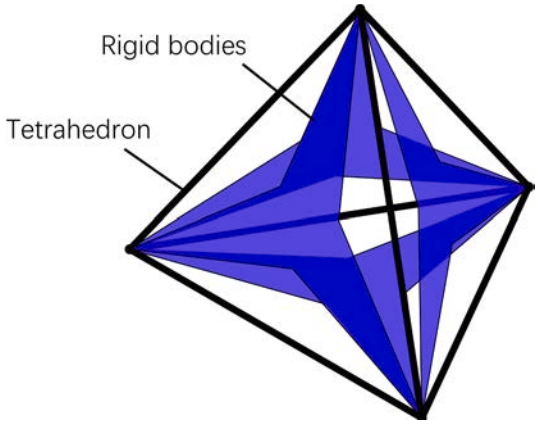

Fig. 14. A tetrahedron build with rigid bodies.

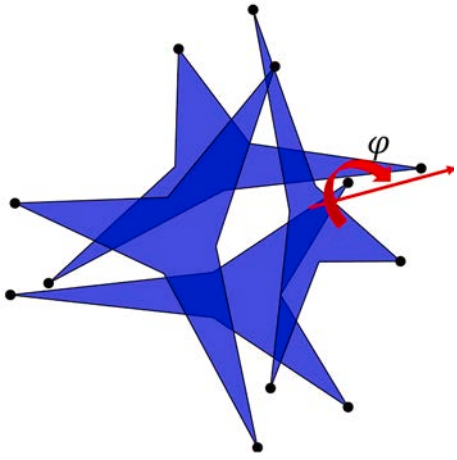

Fig. 15. Rotation of the rigid bodies.

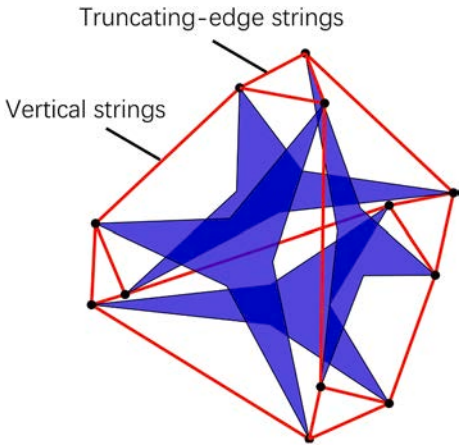

Fig. 16. Initial configuration of a tetrahedron tensegrity with rigid bodies.

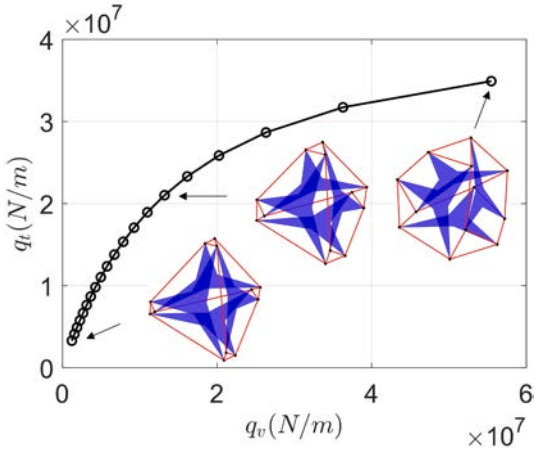

Fig. 17. Form-finding solution of tetrahedron generalized tensegrity.

$$\boldsymbol{N} = \begin{bmatrix} 0.8955 & -0.8365 & 0.0310 & 2.0000 & -2.0000 & 0.0094 & 1.0000 & -1.0000 & 0.0300 \\ 0.3221 & 0.3204 & -1.1787 & 1.0000 & 1.0000 & -2.3218 & -3.0000 & -3.0000 & -0.1787 \\ 0 & 0 & 0 & 0 & 0 & 0 & 0 & 0 & 0 \end{bmatrix}. \tag{85}$$

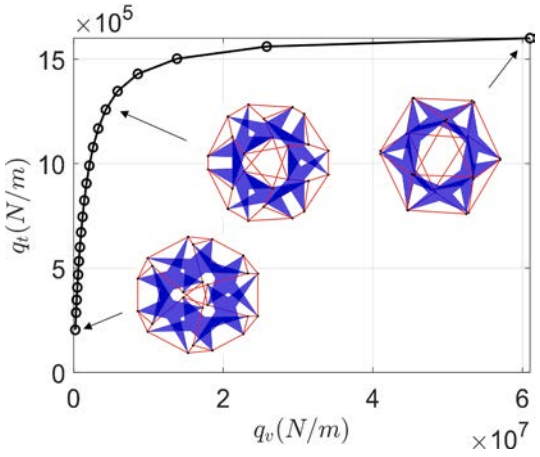

Fig. 18. Form-finding solution of hexahedron generalized tensegrities.

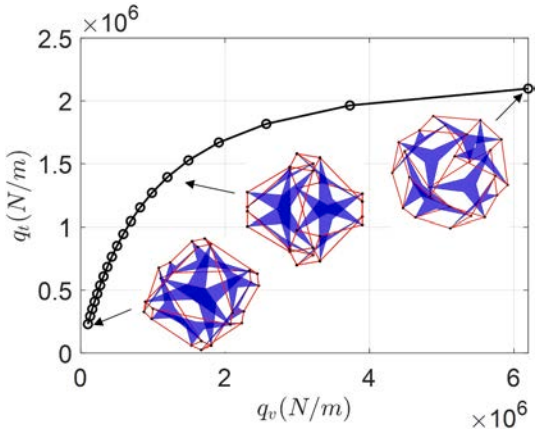

Fig. 19. Form-finding solution of octahedral generalized tensegrities.

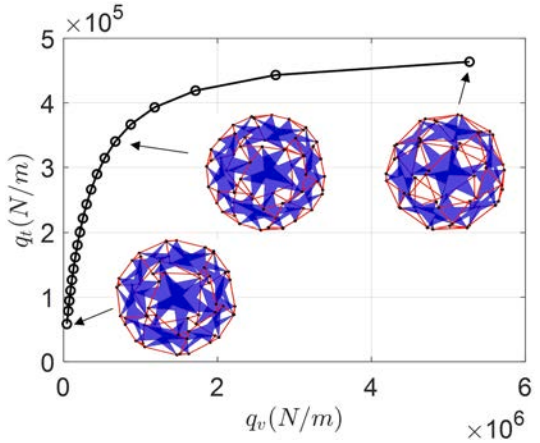

Fig. 20. Form-finding solution of dodecahedral generalized tensegrities.

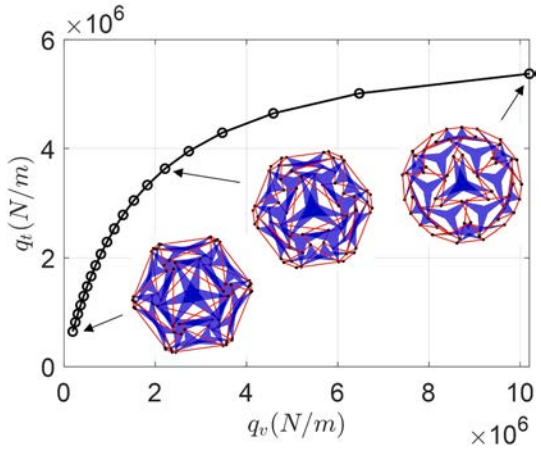

Fig. 21. Form-finding solution of icosahedral generalized tensegrities.

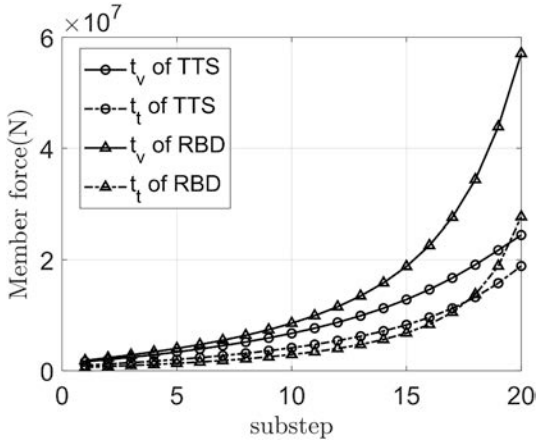

Fig. 22. Comparison of member forces.

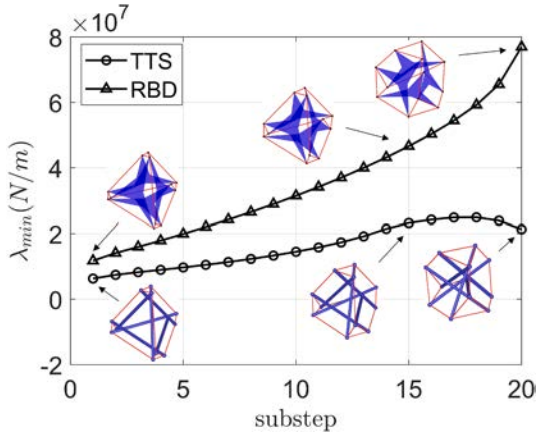

Fig. 23. Comparison of the minimal eigenvalue of the tangent stiffness matrix.

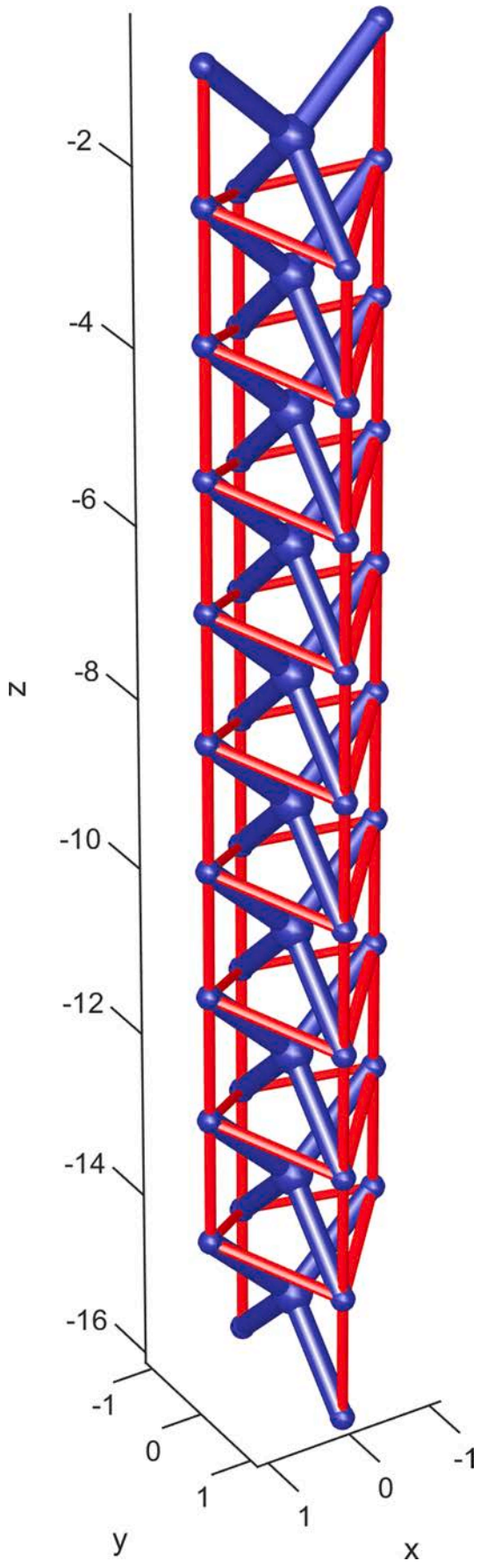

Fig. 24. The initial configuration of the tensegrity spine.

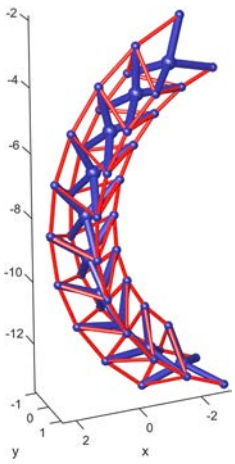

Fig. 25. C-shape, achieved by changing the rest length of the strings on one side linearly.

From Eq. (13), the connectivity matrix $\boldsymbol{C} \in \mathbb{R}^{5\times 8}$ in initial configuration is:

$$\boldsymbol{C} = \begin{bmatrix} -1 & 0 & 0 & 1 & 0 & 0 & 0 & 0 & 0 \\ 0 & -1 & 0 & 0 & 1 & 0 & 0 & 0 & 0 \\ 0 & 0 & -1 & 0 & 0 & 1 & 0 & 0 & 0 \\ 0 & 0 & 0 & 0 & 0 & -1 & 1 & 0 & 0 \\ 0 & 0 & 0 & 0 & 0 & -1 & 0 & 1 & 0 \end{bmatrix}. \tag{86}$$

From Eq.(15), one can get the structure element matrix $\boldsymbol{H} \in \mathbb{R}^{3\times 5}$:

$$\boldsymbol{H} = \begin{bmatrix} 1.1045 & -1.1635 & -0.0216 & 0.9906 & -1.0094 \\ 0.6779 & 0.6796 & -1.1430 & -0.6782 & -0.6782 \\ 0 & 0 & 0 & 0 & 0 \end{bmatrix}. \tag{87}$$

From Eq. (65), the equilibrium matrix for tensegrity with rigid bodies $\boldsymbol{A}_r \in \mathbb{R}^{9\times 5}$ can be calculated:

$$\boldsymbol{A}_r = \begin{bmatrix} 0 & 0 & -0.0189 & -0.8251 & 0.8300 \\ 0 & 0 & -0.9998 & 0.5649 & 0.5577 \\ 0 & 0 & 0 & 0 & 1 \\ -0.8523 & 0.8635 & 0.0189 & 0 & 0 \\ -0.5231 & -0.5044 & 0.9998 & 0 & 0 \\ 0 & 0 & 0 & 0 & 0 \\ 0 & 0 & 0 & 0 & 0 \\ 0 & 0 & 0 & 0 & 0 \\ -0.0259 & 0.0060 & 0.0199 & 0 & 0 \end{bmatrix}. \tag{88}$$

Singular value decomposition of equilibrium matrix reveals the rank of $\boldsymbol{A}_r$ is $r = 4$. That is to say, the structure has $\mathrm{s} = 5 - \mathrm{r} = 1$ self-stress mode and $\mathrm{m} = 9 - r = 5$ mechanism modes. The null space of the equilibrium matrix $\boldsymbol{A}_r$ gives the self-stress mode $\boldsymbol{V}_2$ of the system:

$$\boldsymbol{V}_2 = [-0.4678 \quad -0.4514 \quad -0.4725 \quad -0.4166 \quad -0.4250]^T. \tag{89}$$

The left null space of the equilibrium matrix $\boldsymbol{A}_r$ gives the mechanism modes $\boldsymbol{W}_2$ of the system:

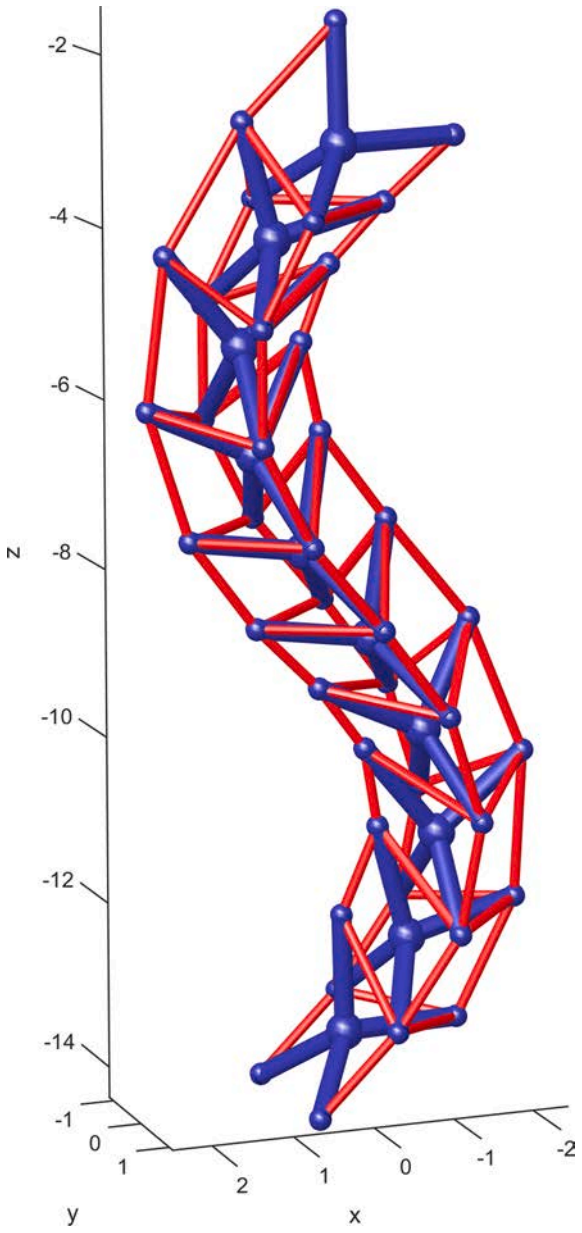

Fig. 26. S-shape, achieved by changing the rest length of the strings on two sides sinusoidally but with different phases.

$$\boldsymbol{W}_2 = \begin{bmatrix} 0 & 0 & 0 & 0 & 0 \\ 0 & 0 & 0 & 0 & 0 \\ -0.6024 & 0 & 0 & 0 & -0.7982 \\ 0.0147 & 0 & 0 & 0 & -0.0111 \\ 0.0156 & 0 & 0 & 0 & -0.0118 \\ 0 & 1.0000 & 0 & 0 & 0 \\ 0 & 0 & 1.0000 & 0 & 0 \\ 0 & 0 & 0 & 1.0000 & 0 \\ -0.7970 & 0 & 0 & 0 & 0.6021 \end{bmatrix}. \tag{90}$$

Each column of $\boldsymbol{W}_2$ represent a mechanism mode. The five mechanism mode shapes are plotted in Fig. 7, where the dashed line and solid lines are the equilibrium configuration and the deformed shape of the mechanism, respectively. The 1st, 3rd, and 4th mechanism modes correspond to the rotation motion of the rigid body about the X, *Y*, *Z*-axis. The 2nd mechanism mode contains the translation motion of the rigid body in the *Z*-axis, and the 5th mode contains the translation of free node in the *Z*-axis, translation of mass center in *X*, *Y*-axis, and rotation of rigid body by *Z*-axis.

The mechanism mode is the null space of the material stiffness matrix which means there is no elongation of the axial member in the mechanism mode. For tensegrity systems, the mechanism mode can be stiffened by prestress. The system's stability can be checked by the product force [42,43] or by the positive-definite of tangent stiffness matrix [28,44]. The eigenvalue of the tangent stiffness matrix $\boldsymbol{K}_{TR}$ is plotted in Fig. 8, we can see that all the eigenvalues of the tangent stiffness matrix are positive, which means the mechanism mode is stiffened by prestress.

The deformed shape corresponding to the first four eigenvalues of the tangent stiffness matrix is plotted in Fig. 9. The dotted line is the equilibrium configuration, and the solid line is the deformed shape. As we can see, the 1st and 4th mode shapes contain out-of-plane deformation, while the 2nd and 3rd mode shapes contain pure planer deformation.

5.2.3. *Tensegrity table*

This example presents a self-equilibrated tensegrity table composed of two rigid bodies and four strings. Fig. 10 is the initial configuration. The rest length of the strings is set to be 0.3 times of present length, which is $\boldsymbol{l}_0 = 0.3\boldsymbol{l}$, to generate prestress of the structure. Fig. 11 shows the equilibrium configuration of the form-finding result.

The prestress mode of the equilibrium matrix is:

$$\boldsymbol{V}_2 = [0.2887 \quad 0.2887 \quad 0.2887 \quad 0.8660]^T. \tag{91}$$

The first three values reveal that the forces of the three long strings are the same. And the fourth value indicates that the short string's inner force is three times that of the long string at an equilibrium state.

Fig. 12 is the eigenvalue of the tangent stiffness matrix. The first six eigenvalues correspond to the rigid body modes of the structure. Fig. 13 shows the mode shapes of the tensegrity table, where mode 6 is a pure rotational mode with zero stiffness. The 7th mode is the most flexible one, which involves the relative rotation of two rigid bodies about the Z-axis.

5.2.4. *Spherical tensegrity*

This example presents a spherical tensegrity composed of multiple rigid bodies in which all nodes lie on the vertices of a regular polyhedron. Truncated tensegrity is the simplest way to build spherical tensegrities, and there are a few studies about this topic [39,45,46,47]. In this example, we propose a novel method to build spherical tensegrity with rigid bodies and study the equilibrium condition of the structure. Here we use the tetrahedron as an example to illustrate the step-by-step procedure to generate a spherical tensegrity with a rigid body, the equilibrium configuration, and the member force of all the other regular polyhedrons tensegrity with rigid bodies.

In Fig. 14, four rigid bodies are initially placed in the plane of the tetrahedron, and rigid body nodes are placed in the tetrahedron's vertices. Each rigid body is rotated by an angle φ about the normal line of the plane to generate a new shape with 12 nodes, as shown in Fig. 15.

If we connect the nodes of the rigid bodies in the initial configuration, there will be 12 truncating-edge strings and 6 vertical strings, as in Fig. 16. To prestress the spherical tensegrity, the rest length of the vertical strings is set to [0.1,0.8] times its present length while truncating-edge strings are identical to its present length. The form-finding result of a truncated tetrahedral generalized tensegrity is shown in Fig. 17. The force density of truncating-edge strings and vertical strings are respectively q_t and q_v. We can observe that the force density of both truncating-edge strings and vertical strings increases as the rest length of vertical strings decreases.

The form-finding result for other regular polyhedron shapes, including hexahedron, octahedral, dodecahedral, and icosahedral generalized tensegrities, are shown in Figs. 18-21.

In our example, to make a fair comparison between the TTS (traditional tensegrity structure) and RTS (rigid-body tensegrity structure). We first set the initial nodal coordinate of the TTS and RTS to be identical. To take the consideration of rigid bodies, we assign the axial stiffness of bars to be 1000 times the strings. The rest length of the vertical strings is set to be [0.1,0.8] times its present length, while truncating-edge strings and bars are identical to their present length in the initial configuration. In the form-finding process, we shorten the rest length of the vertical strings in the TTS and RTS to have an equal length at each substep. The member forces in the equilibrium configuration at each substep are shown in Fig. 22. We can see that the member force of vertical strings in RTS increases a lot more than that of TTS. It is because the TTS has more freedom to deform and release the increasing strain energy. Moreover, the stiffness in the TTS and RBD are also different. As shown in Fig. 23, the minimal eigenvalue of RTS is more than two times the TTS structure at each substep.

5.2.5. Tensegrity spine

As the last example, we study a tensegrity spine [48,49] composed of multiple rigid bodies. Fig. 24 is the initial configuration of the tensegrity spine. The tensegrity spine comprises 10 rigid body units, and the 10 rigid bodies are connected by four groups of vertical side strings and nine groups of diagonal strings.

The rest length of all the diagonal strings is set to 0.9 times the present length. The rest length of the three groups of vertical side strings is set to 0.9 times the present length, while the rest length of the other group of vertical side strings is set to 0.6 times the present length. The equilibrium configuration calculated by the form-finding method is shown in Fig. 25.

The rest length of two groups of vertical side strings in the opposite positions is 0.9 times the length in the initial shape, while the rest length of the other two groups of vertical side strings varies from 0.5 to 1.1 times the length in the initial shape. The equilibrium configuration calculated by the form-finding method is shown in Fig. 26.

6. Conclusions

During the past few decades, pure bar-string network tensegrity has shown its great strength in designing efficient structures in many aspects. However, to embrace a much more general problem of system design using the tensegrity paradigm, rigid bodies must be included. Aiming at extending the ability to analyze rigid body tensegrities with analytical tools, this paper formulates the nonlinear equilibrium equation of the rigid body tensegrity in an explicit form in terms of the minimal coordinate. To get the insight of each structure member, we derived its equivalent form, which is a linear equation in terms of the force vector. Then, we also provide the compatibility equation and tangent stiffness matrix of the system for stability analysis. Finally, an efficient form-finding method of the rigid body tensegrity is given based on the equilibrium and stiffness equations. In the proposed form-finding method, a modified tangent stiffness matrix and line search algorithm are used to guarantee the result to fast converge to a stable equilibrium configuration. It is also shown that the nonlinear equilibrium equations of the general tensegrity degenerate to the ones of the traditional tensegrity without rigid bodies. Four numerical examples are given to prove the accuracy and efficiency of the developed principles. Results show that the developed principles can deal with form-finding from a non-equilibrium state, find the prestress and mechanism modes, and conduct stiffness studies.

CRediT authorship contribution statement

Shuo Ma: Conceptualization, Methodology, Software, Validation, Writing – original draft. **Muhao Chen:** Conceptualization, Methodology, Software, Validation, Writing – original draft. **Zhangli Peng:** Conceptualization, Methodology, Writing – review & editing. **Xingfei Yuan:** Conceptualization, Methodology, Writing – review & editing, Supervision. **Robert E. Skelton:** Conceptualization, Methodology, Writing – review & editing, Supervision.

Declaration of Competing Interest

The authors declare that they have no known competing financial interests or personal relationships that could have appeared to influence the work reported in this paper.

Acknowledgment

The research was supported by the Foundation of Key Laboratory of Space Structures of Zhejiang Province (Grant No. 202102) and the National Natural Science Foundation of China (Grant No. 51878600).

Appendix

Derivation of the cable acceleration.

From Eq.(16), the i th cable's velocity is:

$$\dot{l}_i = \frac{\boldsymbol{h}_i^T}{l_i}\dot{\boldsymbol{h}}_i = \boldsymbol{h}_{n_i}^T\dot{\boldsymbol{h}}_i, \tag{92}$$

where $\boldsymbol{h}_{n_i} = \frac{\boldsymbol{h}_i}{l_i}$ is the i th cable's unit vector. The i th cable's acceleration is:

$$\ddot{l}_i = \dot{\boldsymbol{h}}_{n_i}^T\dot{\boldsymbol{h}}_i + \boldsymbol{h}_{n_i}^T\ddot{\boldsymbol{h}}_i. \tag{93}$$

$\dot{\boldsymbol{h}}_{n_i}$ is the time derivative of the i th cable's unit vector, which can be derived as:

$$\dot{\boldsymbol{h}}_{n_i} = \frac{\dot{\boldsymbol{h}}_i l_i - \boldsymbol{h}_{n_i}^T\dot{\boldsymbol{h}}_i\boldsymbol{h}_i}{l_i^2} = \frac{\left(\boldsymbol{I}_3 - \boldsymbol{h}_{n_i}^T\boldsymbol{h}_{n_i}\right)}{l_i}\dot{\boldsymbol{h}}_i = \frac{\boldsymbol{P}_{hn_i}}{l_i}\dot{\boldsymbol{h}}_i, \tag{94}$$

where $\boldsymbol{P}_{hn_i} = \boldsymbol{I}_3 - \boldsymbol{h}_{n_i}\boldsymbol{h}_{n_i}^T \in \mathbb{R}^{3\times 3}$ is a symmetric matrix. Therefore, using Eqs.(43), (14), and (94), the first term of Eq.(93) can be rewritten as:

$$\dot{\boldsymbol{h}}_{n_i}^T\dot{\boldsymbol{h}}_i = \dot{\boldsymbol{h}}_i^T\frac{\boldsymbol{P}_{hn_i}^T}{l_i}\dot{\boldsymbol{h}}_i = \dot{\boldsymbol{U}}^T\boldsymbol{G}^T\left(\boldsymbol{C}_i^T\otimes\boldsymbol{I}_3\right)\frac{\boldsymbol{P}_{hn_i}}{l_i}(\boldsymbol{C}_i\otimes\boldsymbol{I}_3)\boldsymbol{G}\dot{\boldsymbol{U}}. \tag{95}$$

The acceleration of the k th node on the j th rigid body is:

$$\ddot{\boldsymbol{n}}_{qjk} = \ddot{\boldsymbol{n}}_{cj} + \dot{\boldsymbol{\omega}}_j\times\boldsymbol{r}_{jk} + \boldsymbol{\omega}_j\times\left(\boldsymbol{\omega}_j\times\boldsymbol{r}_{jk}\right). \tag{96}$$

According to Eqs.(9) and (14), the second term of Eq.(93) is:

$$\boldsymbol{h}_{n_i}^T\ddot{\boldsymbol{h}}_i = \boldsymbol{h}_{n_i}^T(\boldsymbol{C}_i\otimes\boldsymbol{I}_3)\ddot{\boldsymbol{n}} = \boldsymbol{h}_{n_i}^T(\boldsymbol{C}_i\otimes\boldsymbol{I}_3)\left(\boldsymbol{E}_{n_a}\ddot{\boldsymbol{n}}_a + \sum_{j=1}^{m}\sum_{k=1}^{z_i}\boldsymbol{E}_{n_{qjk}}\ddot{\boldsymbol{n}}_{qjk}\right). \tag{97}$$

Substitute Eq.(96) into the second term of Eq.(97), we have:

$$\begin{aligned}\boldsymbol{h}_{n_i}^T(\boldsymbol{C}_i\otimes\boldsymbol{I}_3)\boldsymbol{E}_{n_{qjk}}\ddot{\boldsymbol{n}}_{qjk} &= \boldsymbol{z}_{ijk}^T\begin{bmatrix}\boldsymbol{I}_3 & \left(-\boldsymbol{r}_{jk}\right)^{\times}\end{bmatrix}\begin{bmatrix}\ddot{\boldsymbol{n}}_{cj}\\ \dot{\boldsymbol{\omega}}_j\end{bmatrix} + \begin{bmatrix}\dot{\boldsymbol{n}}_{cj}^T & \boldsymbol{\omega}_j^T\end{bmatrix}\begin{bmatrix}\boldsymbol{0}_{3\times3} & \boldsymbol{0}_{3\times3}\\ \boldsymbol{0}_{3\times3} & \boldsymbol{z}_{ijk}^{\times}\boldsymbol{r}_{jk}^{\times}\end{bmatrix}\begin{bmatrix}\dot{\boldsymbol{n}}_{cj}\\ \boldsymbol{\omega}_j\end{bmatrix} = \boldsymbol{z}_{ijk}^T\begin{bmatrix}\boldsymbol{I}_3 & \left(-\boldsymbol{r}_{jk}\right)^{\times}\boldsymbol{B}_j\end{bmatrix}\ddot{\boldsymbol{U}}_j + \dot{\boldsymbol{U}}_j^T\begin{bmatrix}\boldsymbol{0} & \boldsymbol{0}\\ \boldsymbol{0} & \boldsymbol{B}_j^T\boldsymbol{z}_{ijk}^{\times}\boldsymbol{r}_{jk}^{\times}\boldsymbol{B}_j\end{bmatrix}\dot{\boldsymbol{U}}_j\\ &= \boldsymbol{h}_{n_i}^T(\boldsymbol{C}_i\otimes\boldsymbol{I}_3)\boldsymbol{E}_{n_{qjk}}\overline{\boldsymbol{G}}_{jk}\boldsymbol{E}_{Uj}^T\ddot{\boldsymbol{U}} + \dot{\boldsymbol{U}}^T\boldsymbol{E}_{Uj}\begin{bmatrix}\boldsymbol{0} & \boldsymbol{0}\\ \boldsymbol{0} & \boldsymbol{B}_j^T\boldsymbol{z}_{ijk}^{\times}\boldsymbol{r}_{jk}^{\times}\boldsymbol{B}_j\end{bmatrix}\boldsymbol{E}_{Uj}^T\dot{\boldsymbol{U}},\end{aligned} \tag{98}$$

where $\boldsymbol{z}_{ijk}$ is:

$$\boldsymbol{z}_{ijk} = \left(\boldsymbol{h}_{n_i}^T(\boldsymbol{C}_i\otimes\boldsymbol{I}_3)\boldsymbol{E}_{n_{qjk}}\right)^T. \tag{99}$$

Substitute Eq.(98) into Eq.(97), $\boldsymbol{h}_{n_i}^T\ddot{\boldsymbol{h}}_i$ can be rewritten explicitly with $\dot{\boldsymbol{U}}$ and $\ddot{\boldsymbol{U}}$:

$$\boldsymbol{h}_{n_i}^T\ddot{\boldsymbol{h}}_i = \boldsymbol{h}_{n_i}^T(\boldsymbol{C}_i\otimes\boldsymbol{I}_3)\left(\boldsymbol{E}_{n_a}\boldsymbol{E}_{U_a}^T + \sum_{j=1}^{m}\sum_{k=1}^{z_i}\boldsymbol{E}_{n_{qjk}}\overline{\boldsymbol{G}}_{jk}\boldsymbol{E}_{Uj}^T\right)\ddot{\boldsymbol{U}} + \sum_{j=1}^{m}\sum_{k=1}^{z_i}\dot{\boldsymbol{U}}^T\boldsymbol{E}_{Uj}\begin{bmatrix}\boldsymbol{0} & \boldsymbol{0}\\ \boldsymbol{0} & \boldsymbol{B}_j^T\boldsymbol{z}_{ijk}^{\times}\boldsymbol{r}_{jk}^{\times}\boldsymbol{B}_j\end{bmatrix}\boldsymbol{E}_{Uj}^T\dot{\boldsymbol{U}} = \boldsymbol{B}_{r_i}\ddot{\boldsymbol{U}} + \dot{\boldsymbol{U}}^T\boldsymbol{F}_i\dot{\boldsymbol{U}}, \tag{100}$$

where $\boldsymbol{F}_i \in \mathbb{R}^{n_U\times n_U}$ is:

$$\boldsymbol{F}_i = \sum_{j=1}^{m}\sum_{k=1}^{z_i}\boldsymbol{E}_{Uj}\begin{bmatrix}\boldsymbol{0} & \boldsymbol{0}\\ \boldsymbol{0} & \boldsymbol{B}_j^T\boldsymbol{z}_{ijk}^{\times}\boldsymbol{r}_{jk}^{\times}\boldsymbol{B}_j\end{bmatrix}\boldsymbol{E}_{Uj}^T. \tag{101}$$

With the Eqs.(94)-(101), Eq.(93) can be rewritten as:

$$\ddot{l}_i = \boldsymbol{B}_{ri}\ddot{\boldsymbol{U}} + \dot{\boldsymbol{U}}^T\left(\boldsymbol{G}^T\left(\boldsymbol{C}_i^T\otimes\boldsymbol{I}_3\right)\frac{\boldsymbol{P}_{hn_i}}{l_i}(\boldsymbol{C}_i\otimes\boldsymbol{I}_3)\boldsymbol{G} + \boldsymbol{F}_i\right)\dot{\boldsymbol{U}}. \tag{102}$$

Compare Eq.(76) with Eq.(102), the matrix $\boldsymbol{\Omega}_i$ is:

$$\boldsymbol{\Omega}_i = \boldsymbol{G}^T\left(\boldsymbol{C}_i^T\otimes\boldsymbol{I}_3\right)\frac{\boldsymbol{P}_{hn_i}}{l_i}(\boldsymbol{C}_i\otimes\boldsymbol{I}_3)\boldsymbol{G} + \boldsymbol{F}_i. \tag{103}$$

References

[1] Fuller RB. Synergetics: Explorations in the geometry of thinking. Buckminster Fuller: Estate of R; 1982.
[2] Lalvani H. Origins of tensegrity: Views of Emmerich, Fuller and Snelson. Int J Space Struct 1996;11(1). 28p.
[3] Wang Y, Xu X, Luo Y. Topology-Finding of tensegrity structures considering global stability condition. J Struct Eng 2020;146(12).
[4] Wang Y, Xu X, Luo Y. A unifying framework for form-finding and topology-finding of tensegrity structures. Comput Struct 2021;247:106486.
[5] Roth JK, McCarthy TJ. Optimizing compressive load capacity for differing tensegrity geometries. Comput Struct 2021;249:106523.
[6] Wang Y, Xu X, Luo Y. Minimal mass design of active tensegrity structures. Eng Struct 2021;234:111965.
[7] Feng Y, Yuan XF, Samy A. Analysis of new wave-curved tensegrity dome. Eng Struct 2022;250.
[8] Ma S, Chen M, Skelton RE. Design of a new tensegrity cantilever structure. Compos Struct 2020;243:112188.
[9] Liu Y, Bi Q, Yue X, Wu J, Yang B, Li Y. A review on tensegrity structures-based robots. Mech Mach Theory 2022;168:104571.
[10] Paul C, Valero-Cuevas FJ, Lipson H. Design and control of tensegrity robots for locomotion. Ieee T Robot 2006;22(5):944–57.
[11] Veuve N, Sychterz AC, Smith IFC. Adaptive control of a deployable tensegrity structure. Eng Struct 2017;152:14–23.
[12] Kan Z, Peng H, Chen B, Zhong W. Nonlinear dynamic and deployment analysis of clustered tensegrity structures using a positional formulation FEM. Compos Struct 2018;187.
[13] Hrazmi I, Averseng J, Quirant J, Jamin F. Deployable double layer tensegrity grid platforms for sea accessibility. Eng Struct 2021;231.
[14] Zhang J, Ohsaki M, Rimoli JJ, Kogiso K. Optimization for energy absorption of 3-dimensional tensegrity lattice with truncated octahedral units. Compos Struct 2021;267:113903.
[15] Rimoli JJ. A reduced-order model for the dynamic and post-buckling behavior of tensegrity structures. Mech Mater 2018;116(SI):146–57.
[16] Pajunen K, Johanns P, Pal RK, Rimoli JJ, Daraio C. Design and impact response of 3D-printable tensegrity-inspired structures. Mater Design 2019;182:107966.
[17] Fabbrocino F, Carpentieri G. Three-dimensional modeling of the wave dynamics of tensegrity lattices ER -. Compos Struct 2017;173:9–16.
[18] Fabbrocino F, Amendola A, Benzoni G, Fraternali F. Seismic application of pentamode lattices. Ing Sismica 2016;33(1–2):62–70.
[19] Amendola A, Fabbrocino F, Feo L, Fraternali F. Dependence of the mechanical properties of pentamode materials on the lattice microstructure 2016:2134–50.
[20] Carpentieri G, Skelton RE, Fraternali F. Minimum mass and optimal complexity of planar tensegrity bridges. Int J Space Struct 2015;30(3–4):221–44.
[21] Laccone F, Malomo L, Froli M, Cignoni P, Pietroni N. Automatic design of cable-tensioned glass shells. Computer Graphics Forum: Wiley Online Library; 2020. p. 260–73.
[22] Levin S, M.. The Tensegrity-Truss as a model for spine mechanics: Biotensegrity. Journal of Mechanics in Medicine & Biology 2002.
[23] Chen B, Jiang H. Swimming performance of a tensegrity robotic fish. Soft Robot 2019;6(4):520–31.
[24] Chen M, Goyal R, Majji M, Skelton RE. Design and analysis of a growable artificial gravity space habitat. Aerosp Sci Technol 2020;106:106147.
[25] Wang R, Parunandi KS, Yu D, Kalathil D, Chakravorty S. Decoupled Data-Based approach for learning to control nonlinear dynamical systems. Ieee T Automat Contr 2021.
[26] Sun J, Song G, Chu J, Ren L. An adaptive bioinspired foot mechanism based on tensegrity structures. Soft Robot 2019;6(6):778–89.
[27] Hangai Y, Wu M. Analytical method of structural behaviours of a hybrid structure consisting of cables and rigid structures. Eng Struct 1999;21(8):726–36.
[28] Wang Y, Xu X, Luo Y. Topology design of general tensegrity with rigid bodies. Int J Solids Struct 2020;202:278–98.
[29] Chen B, Jiang H. Instability results from purely rotational stiffness for general tensegrity structure with rigid bodies. Mech Mach Theory 2022;167:104485.
[30] Nagase K, Skelton RE. Network and vector forms of tensegrity system dynamics. Mech Res Commun 2014;59:14–25.
[31] Kan Z, Song N, Peng H, Chen B, Song X. A comprehensive framework for multibody system analysis with clustered cables: Examples of tensegrity structures. Int J Solids Struct 2021;210–211:289–309.
[32] Kan Z, Peng H, Chen B, Zhong W. A sliding cable element of multibody dynamics with application to nonlinear dynamic deployment analysis of clustered tensegrity. Int J Solids Struct 2018;130–131:61–79.
[33] Li F, Peng H, Yang H, Kan Z. A symplectic kinodynamic planning method for cable-driven tensegrity manipulators in a dynamic environment. Nonlinear Dynam 2021;106(4):2919–41.
[34] Skelton RE, Oliveira MCD. Tensegrity systems. Berlin: Springer; 2011.
[35] Hurtado, JE. Kinematic and kinetic principles 2016.

[36] Shabana A. Dynamics of multibody systems. Cambridge University Press; 2020.
[37] Ma S, Chen M, Skelton RE. Tensegrity system dynamics based on finite element method. Compos Struct 2022;280:114838.
[38] Pellegrino S. Structural computations with the singular value decomposition of the equilibrium matrix. Int J Solids Struct 1993;30(21):3025–35.
[39] Zhang L, Li Y, Cao Y, Feng X. Stiffness matrix based form-finding method of tensegrity structures. Eng Struct 2014;58:36–48.
[40] Armitage, P, Colton, T. Encyclopedia of biostatistics || optimization and nonlinear equations. 2005;10.1002/0470011815.
[41] Tran HC, Lee J. Advanced form-finding of tensegrity structures. Comput Struct 2010;88(3–4):237–46.
[42] Pellegrino S. Analysis of prestressed mechanisms. Int J Solids Struct 1990;26(12):1329–50.
[43] Calladine CR, Pellegrino S. First-order infinitesimal mechanisms. Int J Solids Struct 1991;27(4):505–15.
[44] Zhang JY, Ohsaki M. Stability conditions for tensegrity structures. Int J Solids Struct 2007;44(11–12):3875–86.
[45] Li Y, Feng X, Cao Y, Gao H. A Monte Carlo form-finding method for large scale regular and irregular tensegrity structures. Int J Solids Struct 2010;47(14–15):1888–98.
[46] Yuan X, Ma S, Jiang S. Form-finding of tensegrity structures based on the Levenberg–Marquardt method. Comput Struct 2017;192:171–80.
[47] Zhang LY, Li Y, Cao YP, Feng XQ, Gao H. Self-equilibrium and super-stability of truncated regular polyhedral tensegrity structures: A unified analytical solution. Proceedings of the Royal Society A 2012;468(2147):3323–47.
[48] Zappetti D, Arandes R, Ajanic E, Floreano D. Variable-stiffness tensegrity spine. Smart Mater Struct 2020;29(7):75013.
[49] Sabelhaus AP, Zhao H, Zhu EL, Agogino AK, Agogino AM. Model-predictive control with inverse statics optimization for tensegrity spine robots. Ieee T Contr Syst T 2020;29(1):263–77.